Chinese Herbal Medicines 17 (2025) 352–367

Contents lists available at ScienceDirect

Chinese Herbal Medicines

journal homepage: www.elsevier.com/locate/chmed

Original Article

Amelioration of atherosclerotic complications and dyslipidemia by verbascoside-enriched fraction of *Clerodendrum glandulosum* leaves targeting LDL-R and LXR-mediated reverse cholesterol transport

Puspanjali Khound [a,b], Nonibala Gurumayum [a,b], Rajlakshmi Devi [a,b,*]

[a] *Life Sciences Division, Institute of Advanced Study in Science and Technology (IASST), Paschim Boragaon, Garchuk, Guwahati 781035, India*
[b] *Department of Zoology, Gauhati University, Jalukbari, Guwahati 781014, India*

ARTICLE INFO

Article history:
Received 2 July 2024
Revised 31 October 2024
Accepted 24 February 2025
Available online 25 February 2025

Keywords:
atherosclerosis
cholesterol
dyslipidemia
Clerodendrum glandulosum Lindl.
LDL-R
LXRα
verbascoside

ABSTRACT

Objective: *Clerodendrum glandulosum* is widely used in traditional Chinese and Indian systems of medicine for conditions like hypertension and diabetes. While various pharmacological benefits have been reported, research on its anti-atherosclerotic properties remains limited. Atherosclerosis (AS) is a chronic cardiovascular disease linked to dyslipidemia (DLD) and inflammation. This study aims to identify the bioactive fraction from *C. glandulosum* extract, evaluate its potential against AS and DLD, and explore the molecular mechanisms of cholesterol metabolism.

Methods: Bioactivity-guided fractionation was employed to investigate the bioactivity of *C. glandulosum* by screening biochemical enzyme inhibitory potential. The active fraction was subjected to *in vitro* testing to assess the anti-inflammatory and anti-adhesion properties. The fraction was administered at 50 and 100 mg/kg per os (p.o.) to cholesterol-cholic acid-thiouracil (CCT) diet-induced atherosclerotic Wistar rats. Changes in lipid and antioxidant profiles, inflammatory markers, and cholesterol metabolism pathways were assessed using Western blotting. Histopathological analyses of the aorta, liver, heart, and kidneys were also conducted. Molecular docking was conducted for the verbascoside (VER) and the standard statin, atorvastatin (ATS), for their binding capabilities with the molecular targets considered in this study.

Results: Bioactivity-guided fractionation and screening revealed that ethyl acetate fraction (EAF) contained VER as the principal phytoconstituent. EAF exhibited potent enzyme inhibitory activity, with IC_{50} values of 1.059 mg/mL for pancreatic lipase and 22.48 μg/mL for α-glucosidase. In vitro analysis revealed that EAF significantly lowered cell-to-cell adhesion to 0.57 folds from 2.5 folds in the disease control and normalized the inflammatory cytokines. In CCT-diet-induced rats, elevated serum cholesterol and low-density lipoproteins (LDL) levels (92.1 mg/dL and 78.49 mg/dL, respectively) were reduced to 63.52 mg/dL and 58.51 mg/dL with EAF at 100 mg/kg. EAF at 100 mg/kg reduced oxidized LDL to 53.63 ng/mL compared to 157.1 ng/mL in CCT-diet-fed rats. EAF also restored antioxidant activity by increasing superoxide dismutase and catalase levels to 73.78 and 17.72 U/mg protein, respectively, compared to 42.22 and 9.62 U/mg protein in CCT-diet-fed rats. EAF restored inflammatory cytokines to normal levels. Histological analyses validated the protective benefits of EAF supplementation for the structural integrity of the aorta, liver, heart, and kidney tissues. Western blotting analysis of liver tissues revealed changes in the cholesterol metabolic pathway by upregulating peroxisome proliferator-activated receptor gamma (PPARγ)/liver X receptor alpha (LXRα)/adenosine triphosphate-binding cassette sub-family G member 1 (ABCG1) and low-density lipoprotein receptor (LDL-R) expression. Unlike ATS, molecular docking analyses indicated strong interactions between VER and molecular targets.

Conclusion: EAF prevented DLD and AS by reverse cholesterol transport via the PPARγ/LXRα/ABCG1 pathway, offering potential therapeutic benefits for cardiovascular health.

* Corresponding author.
E-mail address: rajiasst@gmail.com (R. Devi).

https://doi.org/10.1016/j.chmed.2025.02.007
1674-6384/

1. Introduction

Atherosclerosis (AS) is a multifactorial pathological condition affecting the arteries and associated with lipid metabolism problems and inflammation (Bergheanu, Bodde, & Jukema, 2017). Different cell types and components of the vascular system contribute to the development of AS. This condition is pathological to the clinical manifestations of ischemia in distal organs, such as the heart, brain, kidneys, etc. The condition is aggravated by dysbalance in the lipid metabolism due to stress factors and abnormal levels of circulating modified low-density lipoprotein (LDL) cholesterols in the vasculature, which disrupts the normal metabolic process of cholesterol. This often leads to endothelial dysfunction, thereby inducing an inflammatory response and leading to cellular adhesion and plaque formation (Joris, Zand, Nunnari, Krolikowski, & Majno, 1983). On receiving the inflammatory response, the blood monocytes differentiate into phagocytic macrophages that engulf LDL cholesterols and apolipoproteins and convert themselves into atherogenic foam cells, which later deposit in the arterial walls and grow in size to form plaque and subsequently form a fibrous cap. The fibrous cap is formed due to the atherogenic conversion of endothelial-to-mesothelial tissue, which then surrounds the foam cells and decreases the passageway for blood flow (Bergheanu et al., 2017).

Recent research has demonstrated the enormous potential of herbal medicines in preventing LDL oxidation and lowering foam cell production caused by oxidized-LDL (ox-LDL) (Duan, Song, Li, Su, & He, 2023). Therefore, lowering plasma LDLs is a major strategy for lowering the incidence of atherosclerotic complications. The LDL receptor (LDL-R) is a cell surface receptor expressed primarily in the liver and is essential for cholesterol metabolism, as hepatocytes predominantly recognize and eliminate plasma LDL cholesterol by LDL-R endocytosis recycling (Yang et al., 2020). The liver's LDL-R expression influences the amount of LDL absorbed from the blood. An increase in LDL-Rs leads to greater uptake of LDL, resulting in lower plasma LDL levels. On the other hand, activation of liver X receptors (LXRs), in response to high cholesterol levels, leads to the transcriptional upregulation of genes and proteins, such as ATP-binding cassette sub-family A member 1 (ABCA1) and ATP-binding cassette subfamily G member 1 (ABCG1) involved in cholesterol efflux, fatty acid synthesis, and lipid transport, ultimately promoting reverse cholesterol transport (RCT) and reducing intracellular lipid accumulation (Im & Osborne, 2011). It has been reported that by upregulating LDL-R, LXR, ABCA1, and ABCG1, herbal medicines inhibit LDL oxidation and maintain cholesterol homeostasis (He et al., 2023; Li & Glass, 2004; Sut et al., 2022; Xie et al., 2023). *Clerodendrum* spp. belongs to the genus encompassing a wide variety of medicinal and ornamental plants throughout the globe due to their various therapeutic properties, including their ability to treat hypertension, inflammation, and diabetes (Wang, Luan, He, Wang, & Li, 2018). Among the different species of *Clerodendrum*, *Clerodendrum glandulosum* Lindl. (syn. *Clerodendrum colebrookianum* Walp.), is extensively used in the traditional medicine of Northeast India and the Chinese system of medicine for treating hypertension, diabetes, obesity, and other cardiovascular complications, which is scientifically evidenced for its effectiveness (Jadeja, Thounaojam, Ramani, Devkar, & Ramachandran, 2011; Jadeja, Thounaojam, Jain, Devkar, & Ramachandran, 2012; Kalita, Singh, & Khan, 2012; Khound et al., 2024; Nath & Bordoloi, 1991; Yang et al., 2000). Dyslipidemia (DLD) results in the multifactorial aggravation of the cholesterol mechanism, leading to atherogenic complications (Duan et al., 2023). Addressing this issue is imperative at present, as AS contributes to the complex exacerbation of the cholesterol mechanism and acts as the underlying root cause leading to cardiovascular complications. This work aims to provide insight into the amelioration of AS and DLD previously investigated in a few reports (Jadeja, Thounaojam, Ansarullah, Devkar, & Ramachandran, 2010; Jadeja et al., 2011, 2012). However, the specific mechanisms behind the reduction of DLD and AS have not been previously documented. In this work, we have investigated the ameliorative effect of the bioactive fraction from the hydro-methanolic extract of *C. glandulosum* leaves in improving DLD and AS in diet-induced atherosclerotic Wistar rats. We attempted to comprehend the molecular mechanism by which the active fraction contributes to cholesterol metabolism via RCT and cholesterol efflux in ameliorating DLD, inflammation, and AS.

2. Materials and methods

2.1. Chemicals and reagents

We obtained all the chemicals from Sigma Aldrich (St. Louis, MO, USA). The kits for biochemical analysis were sourced from Accurex Biomedical Pvt. Ltd. (Mumbai, India). ELISA kits were purchased from G Biosciences (St. Louis, MO, USA). Cell lines, *viz*., human umbilical vein endothelial cells (HUVEC) and Tohoku Hospital Pediatrics-1 (THP-1) cells, were procured from HiMedia Laboratories Pvt. Ltd. (Mumbai, India) and National Centre for Cell Science (Pune, India), respectively. Antibodies for Western blotting were acquired from Abclonal (Woburn, MA, USA) (ABCG1, LDL-R, β-actin) and Santa Cruz Biotechnology (Dallas, Texas, USA) [LXRα, peroxisome proliferator-activated receptor gamma (PPARγ), and sterol regulatory element binding proteins (SREBP-1)]. HPLC-grade solvents and other reagents were purchased from Merck (Mumbai, India). Standards *viz*. atorvastatin calcium (ATS) (Pharmaceutical Secondary Standard; Certified Reference Material), metformin (≥97%), and verbascoside (VER) (≥99%, HPLC) were purchased from Sigma Aldrich (St. Louis, MO, USA).

2.2. Plant material collection and preparation of phenolic-rich ethyl acetate fraction (EAF)

We collected fresh leaves of *C. glandulosum* from the medicinal plant garden at the Institute of Advanced Study in Science and Technology (IASST) in Assam, India, in the winter (December and January) season. Dr. Chaya Deori from the BSI in Shillong, India, identified the leaves, and a voucher specimen (No. BSI/ERC/Tech/2019/614) was submitted to the Life Sciences Division at IASST for reference. The fresh leaves (6.5 kg) were collected, washed, dried, and ground to obtain 1.3 kg of dry leaf powder. To extract the active compounds, we cold macerated approximately 1 kg of powdered leaves with 5 L (1:5, mass to volume ratio) of 80% methanol–water at room temperature (25 ± 2) °C for three days. This process was repeated three times with fresh solvent each time. The resulting crude extract, hydromethanolic extract (HMEx), was concentrated at (37 ± 2) °C under reduced pressure using a vacuum rotary evaporator (Buchi R210 Labortechnik AG, Flawil, Switzerland). Subsequently, a portion of the HMEx (50 g) was dissolved in 500 mL of distilled water and sequentially fractionated with hexane (500 mL), ethyl acetate (500 mL), and *n*-butanol (500 mL), thrice. The remaining brown aqueous phase was considered the water fraction. All the fractions were concentrated using a vacuum rotary evaporator (Buchi R210 Labortechnik AG, Flawil, Switzerland) and dried using a lyophilizer (LABCONCO, Kansas City, MO, USA) to obtain the following fractions: hexane fraction (HF), 4.57 g; EAF, 23.55 g; *n*-butanol fraction (NBF), 11.98 g; water fraction (WF), 6.85 g. All fractions were stored at −20 °C for further use. Fig. 1 illustrates the study design and framework.

2.3. Enzyme inhibitory study for screening of bioactive fraction

The α-glucosidase and pancreatic lipase enzyme inhibitory assays were performed for the crude extract and all the fractions for screening bioactivity according to the established protocols

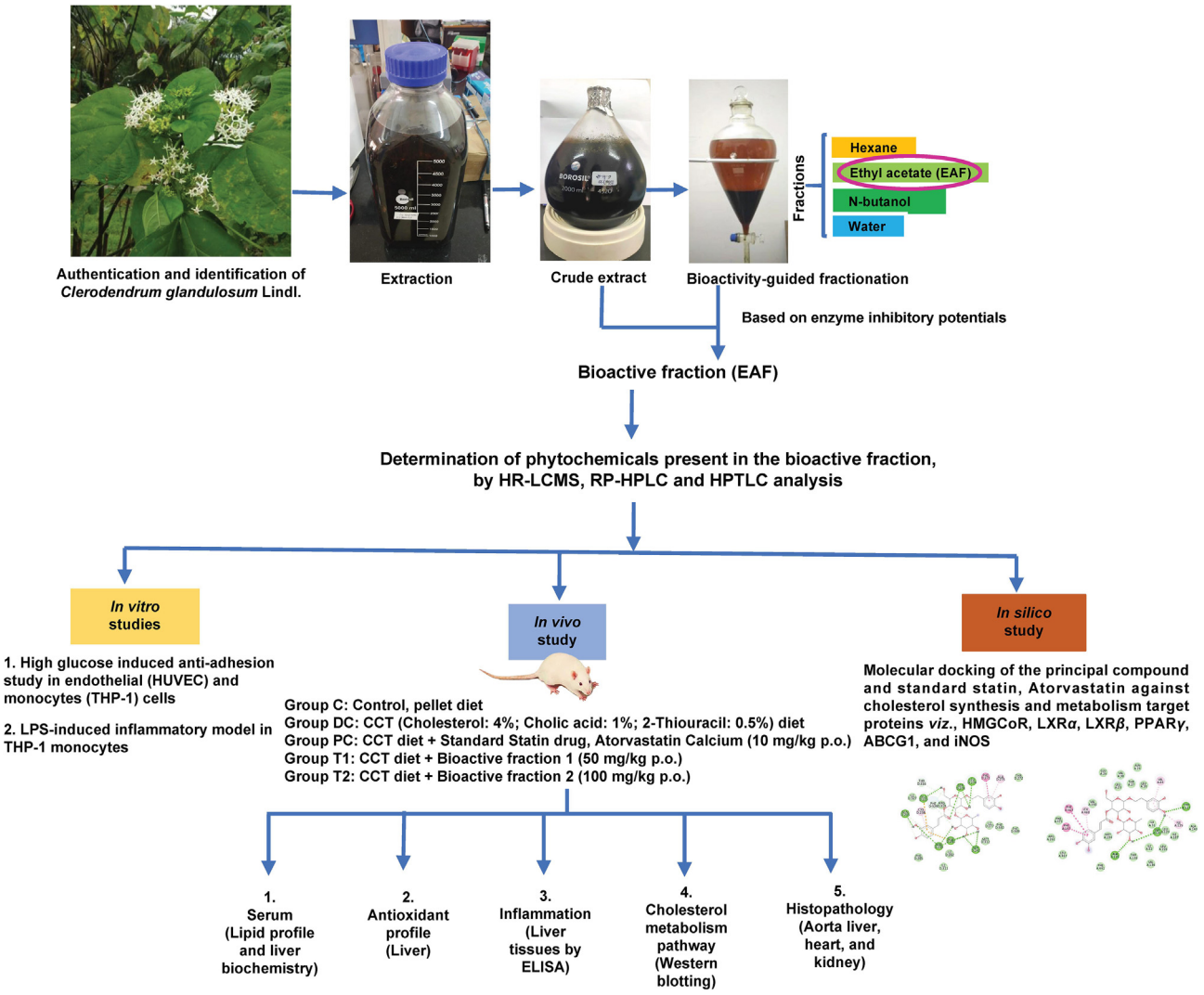

Fig. 1. Illustration of study design and framework.

(Costantino, Brown, & Kelly, 1990; Khound, Sarma, Sarma, Jana, & Devi, 2023; Sharma, Sharma, & Seo, 2005).

2.4. High resolution-liquid chromatography-mass spectrometry (HR-LCMS) analysis

To obtain the phytochemical profile of the EAF of *C. glandulosum* leaf extract, we conducted HR-LCMS analysis using the Q-Exactive Plus Biopharma (Thermo Scientific, Massachusetts, USA). The analysis was performed on a Syncronis C_{18} column (100 mm × 2.1 mm, 1.7 µm) (Thermo Scientific, Massachusetts, USA). A total volume of 250 µL of EAF was injected into the system using a Hamilton syringe (Massachusetts, USA), and the flow rate was maintained at 300 µL/min for 35 min. The solvent system included solvent A of 0.1 % formic acid in Milli-Q water and solvent D of acetonitrile. The electrospray ionization technique was utilized for ionization, providing both positive and negative electrospray ionization. Data acquisition was performed by Thermo Scientific Xcalibur (Version 4.2.28.14), and data processing was conducted by Compound Discoverer 3.2 SP1. Chromatograms were obtained for both positive and negative electrospray ionization modes in mass spectrometry (MS), demonstrating the formation of positive ions ($[M + H]^+$) and negative ions ($[M–H]^-$), respectively, and the mass-to-charge ratio (m/z) values of the ions were obtained along with the suggested name of compounds and their molecular weights by comparing with the mzCloud and ChemSpider databases. Secondary metabolites were identified by analyzing their unique mass fragmentation patterns and mass spectra (Salunke, Wakure, & Wakte, 2023).

2.5. Reverse phase-high-performance liquid chromatography (HPLC)

The HPLC experiments were conducted on a Shimadzu LC-20 AD HPLC system (Mundelein, Illinois, USA) equipped with a prominence photodiode array (PDA) detector. For analytical HPLC, a Discovery RP C_{18} analytical column (10 mm × 4.6 mm, 5 µm) (Merck, Supelco, Darmstadt, Germany) was used with a mobile phase of water and methanol. The flow rate was set at 1 mL/min. The method employed a linear gradient over a total run time of 31 min. Initially, the concentration of water (solvent A) was 100 %, and over a period of 15 min, the concentration of methanol (solvent B) linearly increased to 100 %. Thereafter, a constant flow of 100 % solvent B was maintained for 20 min, and finally, the initial column conditions were restored by 31 min.

2.6. Quantitative analysis of VER by HPLC-PDA

To assess the bioactive fraction EAF, we carried out a quantitative analysis using HPLC. VER, a compound of interest, was used for this analysis. Initially, a standard stock solution of VER was prepared at a

concentration of 1 mg/mL. From this stock solution, various dilutions were made to achieve the desired test concentrations.

To determine the amount of VER in the enriched fraction, we constructed a standard calibration curve (Fig. S1) by plotting the concentration of the compound against the corresponding peak area detected by the HPLC. This calibration curve allowed for the quantitative estimation of VER in the enriched fraction. The concentration of VER in the EAF was expressed as mean ± SD (mg/g), representing the average concentration of the compound along with its standard deviation per gram of the fraction.

2.7. High-performance thin-layer chromatography (HPTLC)

The crude extract, NBF, and EAF were applied in volumes of 5 μL onto a clean thin layer chromatography (TLC) plate (Merck, Supelco, Darmstadt, Germany) measuring 10 × 10 cm. This application was facilitated using the CAMAG LINOMAT 5 with a nitrogen gas flow at 200 nL/s. The TLC plate was then moved to a running chamber that had been lined with filter paper saturated with a mobile phase consisting of ethyl acetate, water, acetic acid, and formic acid in a ratio of 8.5:0.5:0.5:0.5. After the chromatographic run was completed, the plate was removed from the mobile phase and allowed to air dry for 5 min. We used the CAMAG TLC scanner 2 to visualize the plates, and further analysis was conducted using the CAMAG TLC scanner 4. The obtained data were collected using the VisionCATS software. To ensure the method's accuracy, we compared the R_f value and UV spectrum of both the samples and the standard VER.

2.8. In vitro analyses

2.8.1. High-glucose treated adhesion of THP-1 monocytes to human umbilical vein endothelial cells (HUVEC)

Intercellular adhesion was induced by culturing endothelial and monocyte cells in high glucose (25 mmol/L). A monolayer of HUVEC was allowed to grow, and THP-1 monocyte cells labeled with a fluorescent dye, 5-chloromethyl fluorescein diacetate (Thermo Fisher Scientific, Waltham, MA, USA), were then added and incubated for an hour. Prior to the high glucose treatment, the cells were pre-treated with EAF at concentrations of 12.5, 25, and 50 μg for three hours. Afterward, the cells were washed, and measurements were taken at an excitation/emission spectra of 492/517 nm using a Varioskan LUX multimode microplate reader (Thermo Fisher Scientific, Waltham, MA, USA).

2.8.2. LPS-induced inflammation in THP-1 monocytes

Phorbol myristate acetate (Sigma, St. Louis, MO, USA), 50 ng was used to stimulate the differentiation of THP-1 monocytic cells into macrophages. The resulting macrophages were then pre-treated with EAF (25, 50, and 75 μg/mL), as well as a positive control, metformin (60 μmol/mL), for three hours prior to being exposed to lipopolysaccharide (LPS) (Sigma, St. Louis, MO, USA) at a concentration of 10 μmol/mL. This LPS treatment induced an inflammatory response, leading to an increase in pro-inflammatory cytokines (IL-1β, IL-6, and TNF-α) and a decrease in the anti-inflammatory cytokine (IL-10) levels. Additionally, the presence of inducible nitric oxide synthase (iNOS) expression was determined, as it serves as an indicator of inflammation. Protein expressions were analyzed using competitive sandwich enzyme-linked immunosorbent assay (ELISA) kits provided by G Biosciences (St. Louis, MO, USA).

2.9. In vivo analyses

2.9.1. Acute toxicity study

An acute toxicity study was conducted following the Organization for Economic Cooperation and Development Guidelines 315 using Swiss albino female mice weighing (30 ± 2.01) mg. The mice were administered EAF orally at doses of 1 000 and 2 000 mg/kg p.o. and were closely monitored for behavioral changes and signs of toxicity over a period of 14 d.

2.9.2. Experimental animals

Wistar albino rats weighing 180–200 g were housed in a controlled environment, with a temperature of (25 ± 2) °C and humidity of (55 ± 5)%. They were exposed to a 12-hour light/dark cycle and provided unlimited access to purified water and a standard laboratory chow diet. The experiments were conducted during the light phase and received ethical clearance from the Institutional Animal Ethics Committee (IASST/IAEC/2021–22/06 dated 20.09.2022).

2.9.3. Induction of AS

Male Wistar albino rats, aged 12 weeks, were acclimated for one week before the study. The animals were fed a standard pellet diet [M/s Amrut Laboratory Animal Feeds, India with composition-protein: 18.9%, fat (ether extract): 11.0%, fat (acid hydrolysis): 11.2%, crude fiber: 2.2%, nitrogen-free extracts: 52.2% & total digestible nutrients: 88.1%] and experimental DLD was induced by feeding the rats a CCT [Cholesterol: 4% (C8667, Sigma ≥ 99%, St. Louis, MO, USA); cholic acid: 1 % (C2158000, Sigma, St. Louis, MO, USA); 2-thiouracil: 0.5% (27750, Sigma ≥ 99%, St. Louis, MO, USA)] diet, as described by Joris et al. (Joris et al., 1983). Following two weeks of administration of the CCT diet, the blood lipid profiles of the rats were evaluated to confirm the presence of DLD, identified as a potential atherogenic factor. Blood samples were collected from the retro-orbital vein.

2.9.4. Experimental design

The animals were divided into five experimental groups (n = 6) with the following treatment interventions: Group I served as the control (C) and received a standard pellet diet (Table S1); Group II, the disease control (DC), was provided with a CCT-diet; Group III, the positive control (PC), was given ATS at a dose of 10 mg/kg p.o. along with a CCT-diet (Table S1); Group IV, labeled treatment 1 (T1), received EAF at a dose of 50 mg/kg p.o. combined with a CCT-diet; and Group V, labeled treatment 2 (T2), was administered EAF at a dose of 100 mg/kg p.o. along with a CCT-diet.

During the treatment period, all rats were provided with a standard diet. The experimental dose of EAF was selected as 1/10th of the dose used in the acute toxicity study. The treatments were administered orally as a suspension, using 0.5% carboxy methyl cellulose (Sigma, St. Louis, MO, USA) in normal saline. The rats were treated with EAF and the standard statin drug, ATS, for six weeks. At the end of the six-week treatment period, which lasted a total of eight weeks, all the rats were fasted overnight for approximately 12 h on the last day prior to anesthesia induction. They were then euthanized using a combination of Ketamine (87 mg/kg) and Xylazine (3 mg/kg) administered intraperitoneally. Blood samples were collected via heart puncture, and aorta, liver, heart, and kidney tissues were obtained for further analysis.

2.9.5. Measurement of body weight index

Body weights were monitored on a weekly basis throughout the study period. The heart, kidney, liver, spleen, and pancreas were dissected, rinsed with normal saline, dried, and weighed accurately to calculate the organ index. The following formula was used for this calculation

$$\text{Organ index (mg/g)} = \frac{\text{Organ weight (mg)}}{\text{Body weight (g)}}$$

2.9.6. Gas chromatography-mass spectrometry (GC–MS) quantification of fecal metabolite composition

Stool samples were collected at the end of the study. The stool sample (10 mg) was suspended in 0.5 mL of methanol, vortexed,

and centrifuged at 10 000 r/min for 15 min. The supernatant was collected. Further, the process is repeated thrice. The supernatant was then dried in a hot air oven at 37 °C overnight. Once completely dried, we added 0.05 mL of methoxamine hydrochloride (15 mg/mL in pyridine) (Sigma, St. Louis, MO, USA) as a derivatization agent and incubated for 90 min. Further, we added 0.05 mL of *N*-methyl-*N*-(trimethylsilyl) trifluoro-acetamide with 1% trimethylchlorosilane (Sigma, St. Louis, MO, USA) and incubated for 30 min at 37 °C. Further, the solution was filtered using 0.22 mm syringe filters, and the filtrate was transferred into a glass insert.

The analysis of stool samples was performed using a GC–MS system (Shimadzu 2010 plus Triple quadrupole 8040, Kyoto, Japan). The system utilized a silica column with dimensions of 30 m length, 0.25 μm film thickness, and 0.25 mm internal diameter 18. Pure helium gas (99.99 %) was employed as the carrier gas at a constant flow rate of 1.69 mL/min during sample injection to facilitate the separation. The temperature program consisted of an initial period at 130 °C for 5 min, followed by an increase of 10 °C per minute until reaching 250 °C, which was maintained for 10 min. The identification of sterols in the derivatized stool samples involved screening their retention time and mass spectral patterns using the National Institute of Standards and Technology library for comparison.

2.9.7. Biochemical estimation of markers in serum

To obtain serum, blood was collected through heart puncture and then centrifuged at 3 000 r/min for 10 min. Liver biochemical markers- aspartate transaminase (AST), alanine aminotransferase (ALT), and alkaline phosphatase (ALP), as well as lipid profiles-triglycerides (TG), total cholesterol (TC), high-density lipoprotein cholesterol (HDL-C), and LDL-C, were evaluated using standard diagnostic kits (Accurex Diagnostics Pvt. Ltd, Mumbai, India) following the manufacturer's instructions.

2.9.8. Measurement of ox-LDL

The measurement of ox-LDL levels was conducted using the Elabscience Biotechnology Inc. ox-LDL kit (Houston, Texas, USA). This kit employs a double-antibody sandwich ELISA technique to accurately assess the level of ox-LDL in the samples.

2.9.9. Preparation of tissue homogenate and analysis of oxidative stress markers

The excised livers and heart tissues were immediately rinsed with ice-cold potassium phosphate buffer saline at a concentration of 0.01 mol/L and a pH of 7.4. Afterward, a 10 % (mass to volume ratio) tissue homogenate was prepared in ice-cold PBS with the same pH level. The homogenate was then centrifugated at 5 000 r/min for 15 min at a temperature of 4 °C to obtain a clear liquid portion known as the supernatant. The total protein content of the supernatant was determined using a bicinchoninic acid kit (Pierce, Thermo Fischer Scientific, Rockford, IL, USA). The endogenous antioxidant status of the liver tissues was monitored by estimation of glutathione (GSH) level as per Ellman's method (Ellman, 1959), superoxide dismutase (SOD) level as per the reported method (Marklund & Marklund, 1974), and catalase level as per the method of Góth (Góth, 1991). Creatine kinase-myoglobin binding (CK-MB) levels in cardiac tissues were determined by an ELISA kit (G Biosciences, St. Louis, MO, USA).

2.9.10. Measurement of inflammatory cytokine expression in liver tissues

Liver tissue from the experimental rats of each group was processed by homogenization in a tissue lysis buffer containing a 1 % protease and phosphatase inhibitor cocktail. The homogenized tissue was then sonicated for 10 s, three times, using a pulse sonicator. After sonication, the samples were centrifuged at 15 000 r/min for 20 min, and the supernatant was collected. Before storage at −20 °C, the protein content of the samples was estimated. To further analyze the protein expressions of IL-1β, IL-6, TNF-α, IL-10, and iNOS, competitive sandwich ELISA kits (G Biosciences, St. Louis, MO, USA) were used.

2.9.11. 3-Hydroxy-3-methylglutaryl coenzyme A (HMG-CoA) reductase activity

An indirect method was used to estimate the activity of HMG-CoA reductase in liver tissue extracts, by measuring the ratio between HMG CoA and mevalonate (Rao & Ramakrishnan, 1975). This method allows for the determination of HMG-CoA reductase activity indirectly. The decrease in activity of HMG CoA reductase leads to a reduction in mevalonate levels, increasing the ratio.

2.9.12. Immunoblotting studies by western blotting

Western blotting was utilized to examine the influence of the bioactive fraction EAF on proteins associated with hepatic cholesterol metabolism (ABCG1, LDL-R, PPARγ, SREBP-1, and LXRα) in liver tissues from various animal groups. The liver homogenate was prepared as mentioned above. Protein quantification was conducted prior to storing the samples at −20 °C. The proteins were separated on a 10% SDS-PAGE gel (Bio-Rad Laboratories, CA, USA) and transferred electrophoretically to a polyvinylidene fluoride membrane (Merck Millipore Ltd., Carrigtwohill, Co Cork, Ireland). The membrane was blocked with 5 % skimmed milk in tris-buffered saline (Sigma-Aldrich, St. Louis, MO, USA) with Tween 20 (Sigma, St. Louis, MO, USA) for 30 min, followed by overnight incubation at 4 °C with the respective primary antibody (1:1 000). Then, the membrane was probed with the relevant secondary antibody (1:2000) for 1 h at room temperature. The immunoblots were developed using a Bio-Rad ChemiDoc system through the chemiluminescence technique. Protein expression levels were normalized against the housekeeping protein β-actin.

2.9.13. Histopathological analyses

Histopathological examinations of the aorta, liver, heart, and kidney tissues were performed. Tissues were washed with 0.9 % normal saline to remove any traces of blood. Tissues were fixed in a 10 % buffered formalin solution (Himedia, Mumbai, India) (prepared in phosphate-buffered saline, pH 7.4). This was followed by dehydration in increasing grades of 70%, 90%, and 100% alcohol, followed by alcohol: xylene (1:1), and thrice in xylene solution until the tissue turns clear. This was followed by paraffin-embedding, where the tissues were transferred to melted paraffin at 60 °C thrice, and blocks were prepared in a block maker (Leica Biosystems, Nussloch, Germany) and cooled using the chiller (Leica, Biosystems, Nussloch, Germany). Blocks were further trimmed, and sections of 5 μm were cut in a rotary microtome (Leica, Biosystems, Nussloch, Germany). Sections were stretched in a water bath (Jain Scientific Glass Works, Ambala, India) maintained at 60 °C, transferred to egg albumin-coated slides, and left in a hot air oven at 60 °C. The sections were stained using routine Haematoxylin & Eosin (H&E) in an automatic tissue processor (Leica, Biosystems, Nussloch, Germany) and mounted in dibutylphthalate polystyrene xylene (Fischer Scientific, Mumbai, India) for observation under the microscope (Leica, Biosystems, Nussloch, Germany) for histopathological changes.

2.10. Molecular docking

Molecular docking of compounds of *C. glandulosum* leaves with target proteins related to cholesterol synthesis and efflux transport metabolism was predicted by PharmMapper and carried out by utilizing a pharmacophore mapping approach. The 3D structures of the compounds were downloaded from PubChem (https://

pubchem.ncbi.nlm.nih.gov/), and the proteins were downloaded from RCSB Protein Data Bank (https://www.rcsb.org/). LXRβ (IPQ9), iNOS (1NSI), HMG-CoA reductase (2Q6C), and PPARγ (1FM6) were suggested protein targets obtained by PharmMapper. LXRα (2ACL), and ABCG1 (7FDV) proteins were also selected for the docking analysis. Molecular docking was carried out using CB Dock 2 (https://cadd.labshare.cn/cb-dock2/index.php), and the target protein–ligand/compound complexes obtained by docking were further visualized and analysed using the software BIOVIA Discovery Studio 2024.

2.11. Statistical analyses

The mean ± standard deviation was used to express all the results. GraphPad Prism 5.0 software was used to perform all the statistical analyses. A One-way analysis of variance (ANOVA) was conducted, followed by Tukey's multiple comparison tests.

3. Results

3.1. EAF indicates efficient enzyme inhibitory potentials

The crude extract and its fractions were screened for their bioactivity using biochemical assays for enzyme inhibition of α-glucosidase and pancreatic lipase by employing enzyme-substrate reactions. It was observed that the EAF exhibited significant ($P < 0.05$) α-glucosidase inhibitory potentials, indicated by its lower IC_{50} of 22.48 ± 0.74 μg/mL, followed by NBF (IC_{50}, 35.38 ± 2.21 μg/mL), crude methanolic extract, HMEx (IC_{50}, 36.34 ± 0.36 μg/mL), and HF (IC_{50}, 402.95 ± 0.36 μg/mL). A similar trend was observed for pancreatic lipase inhibitory potentials, with EAF (IC_{50}, 1.059 ± 0.39 mg/mL) exhibiting significant ($P < 0.05$) bioactivity compared to NBF (IC_{50}, 2.14 ± 0.24 mg/mL) and HMEx (IC_{50}, 1.53 ± 0.64 mg/mL), as shown in Table 1. WF and HF indicated no lipase inhibitory activities. As the EAF indicated higher efficacy for the enzyme inhibitory potentials, it was considered for the phytochemical analysis and further *in vitro* and *in vivo* studies.

3.2. Comprehensive analysis of phytochemical profile of EAF by HR-LCMS analysis

The HR-LCMS analysis was performed to identify the phytocomponents of EAF, and it provided valuable insights into the complex mixture of bioactive compounds present in the fraction. The chromatograms obtained for both positive and negative electrospray ionization modes in mass spectrometry (MS) demonstrated the formation of positive ions ($[M + H]^+$) and negative ions ($[M–H]^-$), respectively, for the determination of mass-to-charge ratio (m/z) values of the samples and were indicated in Tables 2 and 3 and in Fig. 2A and B. This allowed for the identification of a wide range of m/z values for the phytochemicals present in EAF, typically ranging from 180 to 786.

The identified phytochemicals of EAF encompass a diverse array of compounds, including but not limited to VER, isoferulic acid, azelaic acid, apigetrin, luteolin, echinacoside, apigenin, hispidulin,

Table 1
IC_{50} values of enzyme inhibitory assay of *C. glandulosum* leaf, hydro-methanolic extract (HMEx) and fractions, ethyl-acetate fraction (EAF), *n*-butanol fraction (NBF), hexane fraction (HF) and water fraction (WF) and enzyme inhibitory standards.

Sl.No.	Enzyme inhibitory assay	Activity coefficient	HMEx	EAF	NBF	HF	WF	Standard
1	α-Glucosidase	IC_{50} (μg/mL)	36.34 ± 0.36[b]	22.48 ± 0.74[a]	35.38 ± 2.21[b]	402.95 ± 0.36[c]	–	Acarbose 7.73 ± 0.57
2	Pancreatic lipase	IC_{50} (mg/mL)	1.53 ± 0.64[b]	1.059 ± 0.39[a]	2.14 ± 0.24[b]	–	–	Orlistat 0.315 ± 0.011

Results were obtained in mean ± SD for three sets of experiments. Values in rows followed by different letters differ significantly ($P < 0.05$), as assessed by post hoc test (Tukey test).

Table 2
Phytochemical compounds identified in EAF using HR-LCMS technique obtained for positive electrospray ionization.

Peak No.	RT (min)	Observed m/z	Mass error (mDa)	Formula	Proposed molecule	Fragment ions
1	1.238	122.048 09	0.63	$C_6H_6N_2O$	Nicotinamide	123.055, 106.029, 96.044, 80.050
2	1.262	155.094 62	–0.05	$C_8H_{13}NO_2$	Arecoline	156.101, 110.071, 83.049, 70.065, 58.065
3	9.31	478.147 45	–0.13	$C_{23}H_{26}O_{11}$	Calceolarioside B	325.019, 164.042, 163.039
4	9.481	462.079 79	–0.08	$C_{21}H_{18}O_{12}$	Scutellarin	287.054, 163.038
5	11.115	162.031 60	–0.56	$C_9H_6O_3$	7-Hydroxycoumarine	163.038, 145.028, 135.044, 117.035, 107.049
6	10.024	446.085 04	0.29	$C_{21}H_{18}O_{11}$	Genistein 4′-*O*-glucuronide	271.060, 147.043, 71.148
7	11.009	286.047 59	–0.5	$C_{15}H_{10}O_6$	Kaempferol	287.057, 153.019, 69.873
8	11.776	270.052 87	0.19	$C_{15}H_{10}O_5$	Naringenin	271.059, 155.610, 68.998
9	11.359	300.063 16	–0.77	$C_{16}H_{12}O_6$	Diosmetin	301.070, 155.695, 72.192
10	9.316	180.042 16	–0.53	$C_9H_8O_4$	Caffeic acid	181.044, 163.038, 145.028, 135.044, 117.033, 89.038
11	11.891	300.063 16	–0.77	$C_{16}H_{12}O_6$	Hispidulin	301.071, 286.047

Table 3
Phytochemical compounds identified in EAF using HR-LCMS technique obtained for negative electrospray ionization.

Peak No.	RT (min)	Observed m/z	Mass error (mDa)	Formula	Proposed molecule	Fragment ions
1	9.315	624.205 64	0.35	$C_{29}H_{36}O_{15}$	Verbascoside	461.166 5, 179.034, 161.023 4
2	9.708	194.057 23	–3.48	$C_{10}H_{10}O_4$	Isoferulic acid	193.049, 179.029, 158.845
3	9.779	188.104 11	–3.99	$C_9H_{16}O_4$	Azelaic acid	125.095, 123.080, 97.064
4	9.958	432.105 70	0.11	$C_{21}H_{20}O_{10}$	Apigetrin	431.098, 311.054, 269.045, 268.037, 69.867
5	11.035	286.047 83	0.34	$C_{15}H_{10}O_6$	Luteolin	267.030, 197.060, 150.990
6	11.116	786.237 43	0.27	$C_{35}H_{46}O_{20}$	Echinacoside	785.229, 623.198, 461.167, 271.859, 179.034, 161.023, 135.043, 70.196
7	11.775	270.052 93	0.4	$C_{15}H_{10}O_5$	Apigenin	269.045, 225.054, 152.007, 151.002
8	11.88	300.063 34	–0.17	$C_{16}H_{12}O_6$	Hispidulin	299.056, 284.032, 164.010, 70.645, 65.002
9	12.101	328.225 05	0.23	$C_{18}H_{32}O_5$	Corchorifatty acid F	309.206, 229.144, 211.133, 171.101, 85.028

corchorifatty acid F, nicotinamide, arecoline, calceolarioside B, scutellarin, 7-hydroxy coumarin, genistein 4′-*O*-glucuronide, kaempferol, naringenin, and diosmetin. These compounds belong to various secondary metabolite categories, such as phenolics (glycosides, flavonoids, and flavonols), hydroxycinnamic acids, coumarins, and terpenoids.

3.3. Identification and quantification of VER in EAF using RP-HPLC-PDA

The phenolic profile of the bioactive fraction EAF was analyzed using RP-HPLC-PDA analysis. The chromatogram showed a prominent peak (Peak 1) in Fig. 2C. Peak 1 was identified as VER (RT = 16.732) by comparing its retention time (RT) and UV spectrum with those of the authentic commercially available HPLC grade standard (purity > 99.9%), as shown in Fig. 2D. The concentration of VER in the EAF was determined to be 285.592 ± 10.161 μg/mg, accounting for approximately 28.5% of the fraction.

3.4. Verification of VER in EAF by HPTLC analysis

HPTLC was performed to confirm the presence of VER in the crude hydro-methanolic extract and its polar fractions, EAF and NBF. All the samples indicated the presence of VER (R_f = 0.385) when run along with the commercially available VER standard, as shown in Fig. 2E.

3.5. In vitro analyses

3.5.1. EAF reduces endothelial and monocyte cell adhesion induced by high glucose

Glucose at concentrations of 25 mmol/L resulted in the adhesion of endothelial and monocyte cells up to 2.5 folds. Pre-treatment with EAF at concentrations of 12.5, 25, and 50 μg/mL to both endothelial and monocyte cells resulted in a dose-dependent decline in cellular adhesion between the cells, as indicated by the lowered fluorescence intensity in Fig. 3A and respective fold changes of 2.2, 2.1 and 1.7. Pre-treatment with the EAF to the HUVEC cells indicated significant (P < 0.001) inhibition in adhesion with fold change as low as 1.6 and 1.4 for 25 and 50 μg/mL, respectively. Similar results were observed for THP-1 monocyte cells pretreated with EAF at 25 and 50 μg/mL doses, with fold changes of 1.7 and 1.6, respectively.

3.5.2. Effect of EAF on inflammatory cytokines and iNOS modulation in LPS-treated cells

The inflammatory cytokines and iNOS levels were shown in Fig. 3B–E. IL-1β levels were significantly (P < 0.001) elevated on LPS treatment, which was down-regulated effectively by EAF at 50 μg/mL, similar to metformin. IL-10 significantly (P < 0.01) declined in LPS-treated cells. However, pre-treatment with EAF enhanced the IL-10 levels comparable to control. TNF-α levels spiked on treatment with LPS, which declined significantly (P < 0.01) on pre-treatment of the cells with EAF for 3 h before LPS treatment.

Moreover, LPS treatment enhanced the iNOS levels significantly (P < 0.001). Pretreatment with EAF significantly reduced iNOS levels in a dose-dependent manner, similar to those of positive control.

3.6. In vivo analyses

3.6.1. Behavioral assessment and survival rates in Swiss albino mice following EAF administration

The mice showed no abnormal behavior, and 100 % survival was observed after two weeks of treatment. The behavioral changes observed in Swiss albino mice on administration of 1 000 and 2 000 mg/kg EAF p.o. in a single dose for 14 d were shown in Table S2.

3.6.2. Body weight changes and organ index on EAF administration in CCT-diet-fed rats

Body weight changes were monitored, and it was observed that the CCT diet significantly (P < 0.01) increased the body weights of the DC group in a linear fashion. Administration of EAF effectively prevented the elevation in body weight caused by the CCT diet, as shown in Fig. S2A. The organ index indicated a rise in the liver-organ index, resulting in the deposition of cholesterol in the liver due to feeding on a CCT diet (Fig. S2B).

3.6.3. Effect of EAF on fecal metabolite composition in CCT diet-fed rats

The stool samples indicated the presence of cholic acid and cholesterol metabolites such as lithocholic acid, coprostan-3-ol, cholestane-3-ol, etc. The DC group indicated no significant elimination of sterols, indicating disease progression. However, on administration of EAF to CCT-diet-fed rats, there was significant (P < 0.01) elimination of increased coprostan-3-ol and cholestane-3-ol at 50 mg/kg p.o., as shown in Fig. S3. Cholesterol elimination was also elevated significantly compared to the DC and PC groups on administration of EAF (at 50 and 100 mg/kg p.o.) to CCT diet-fed rats in a dose-dependent manner. Lithocholic acid was slightly enhanced in fecal samples after administration of EAF (50 mg/kg p.o.), though it was not significant.

3.6.4. EAF administration normalizes serum biochemical markers

The DC group indicated elevated levels of total cholesterol, LDL-cholesterol, triglycerides, and depletion of HDL-cholesterol in the serum. Total cholesterol levels significantly declined with the administration of EAF in the groups T1 and T2 in a dose-dependent manner; LDL-cholesterol declined, and HDL-cholesterol enhanced significantly on the administration of EAF in a dose-dependent manner (Fig. 4A, B and D). Triglyceride content was normalized on the administration of EAF (Fig. 4C).

Significant normalization was observed in the liver enzymes viz., ALP, ALT, and AST on the administration of EAF, 100 mg/kg p.o., which were unbalanced on the DC group as shown in Fig. 4J–L. The levels were comparable to those of the PC group. Lowered bilirubin and elevated creatinine levels in the DC group were effectively normalized on administration of EAF in a dose-dependent manner, as shown in Fig. 4F and G. Uric acid levels were similar for all the groups (Fig. 4H).

3.6.5. EAF administration lowers oxidation of LDLs caused by CCT-diet

Ox-LDL is correlated to the initiation and progression of AS (Khorrami et al., 2014). Serum ox-LDL concentration indicated the conversion of LDL to ox-LDL formed in the vascular wall and its elevated plasma levels. The DC group administered with CCT-diet elevated the ox-LDL levels in the serum of the rats significantly (P < 0.001). The subsequent treatment with EAF at 50 and 100 mg/kg p.o. in the T1 and T2 groups showed a decline in the oxidation of LDL particles (Fig. 4E).

3.6.6. EAF administration enhances liver antioxidant levels and reduces cardiac biomarkers in CCT-diet-fed rats

Significant enhancement in the liver antioxidant profile was observed on administration of EAF to CCT-diet-fed animals (Fig. 4M–O). Cardiac tissues expressed elevated CK-MB levels in CCT-diet-fed rats, which were significantly (P < 0.001) downregulated on EAF treatment in a dose-dependent manner, as shown in Fig. 4I.

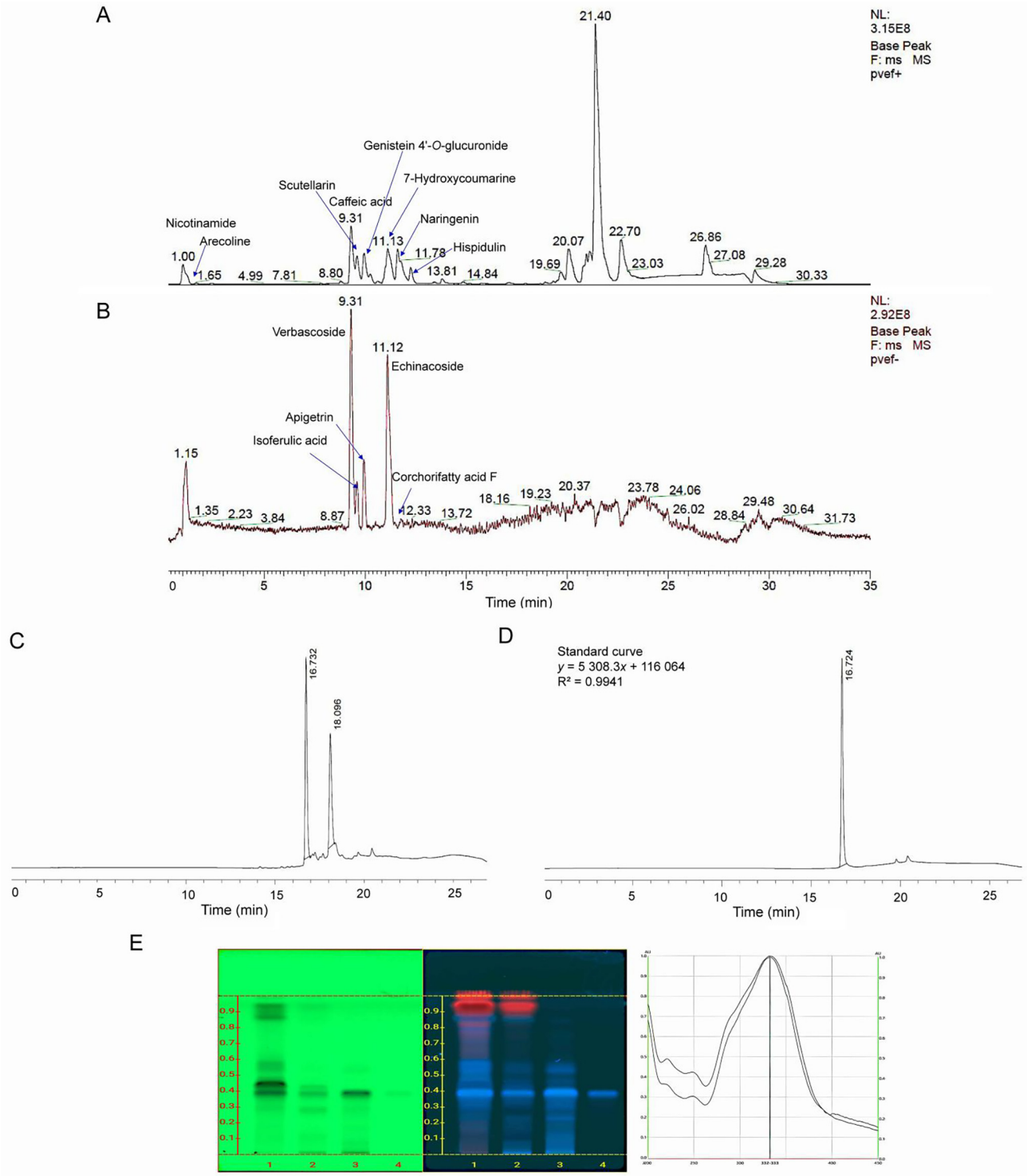

Fig. 2. High-resolution liquid chromatography and mass spectrometry assisted phytochemical profiling of bioactive fraction of *C. glandulosum*. Chromatograms were obtained for (A) positive and (B) negative electrospray ionization; HPLC chromatogram of bioactive fraction, (C) HPLC chromatogram of ethyl acetate fraction (2 mg/mL) indicating two peaks at RT 16.732 & RT 18.096, and (D) HPLC chromatogram of verbascoside standard indicating peak at RT 16.724 obtained at 254 nm wavelength; (E) HPTLC chromatogram developed at 254 nm and 366 nm where Lane 1. Crude hydro-methanolic extract (10 mg/mL), Lane 2. Ethyl acetate fraction (10 mg/mL), Lane 3. *N*-butanol fraction (10 mg/mL), Lane 4. Standard, verbascoside (1 mg/mL) and verbascoside spectrum (to the right).

3.6.7. EAF administration mitigates inflammatory cytokine imbalances induced by CCT diet in rats

CCT diet induced significant expression of pro-inflammatory cytokines *viz*., IL-1β, IL-6, and TNF-α levels and decreased IL-10 levels as indicated by the protein expression performed by ELISA. iNOS was also significantly elevated in CCT-diet-fed rats. EAF ameliorated the changes caused by CCT-diet-induction in a dose-dependent manner, effectively lowering the expression of IL-1β, IL-6, and TNF-α cytokines and upregulating IL-10 levels, as shown in Fig. 5A–D. Elevation in the iNOS levels, induced by the CCT diet, was significantly lowered in the liver tissues on EAF administration (Fig. 5E).

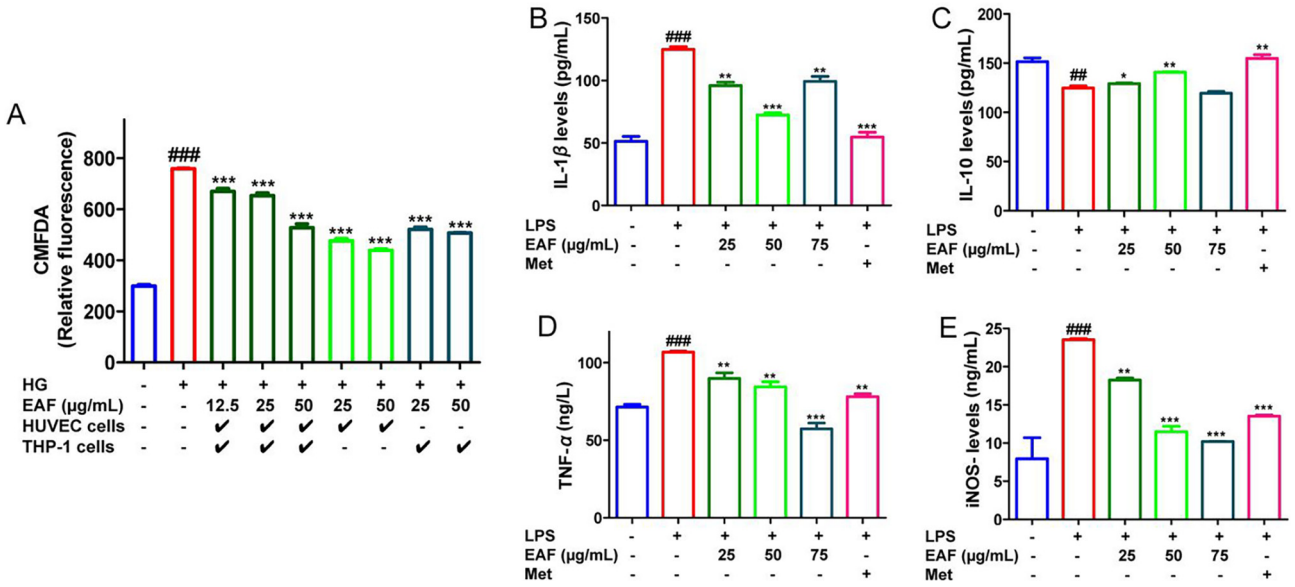

Fig. 3. Graphs indicating (A) anti-adhesion activity by reduction in fluorescence intensity indicative of less monocyte (THP-1)-to-endothelial (HUVEC) cell adhesion, and changes in (B) IL-1β, (C) IL-10, (D) TNF-α (E) iNOS levels in lipopolysaccharide (LPS)-induced differentiation in THP-1 monocytes, pre-treated with ethyl acetate fraction at three concentrations (25 µg/mL, 50 µg/mL, 75 µg/mL), and positive control, metformin (Met), 60 µmol/mL, High glucose (HG), 25 mmol/mL, LPS, 10 µmol/mL. Values are expressed as means ± SD (n = 6). One-way ANOVA was performed, followed by Tukey's Post hoc test. $^{*}P < 0.05$, $^{**}P < 0.01$, $^{***}P < 0.001$ *vs* disease control group; $^{\#\#}P < 0.01$, $^{\#\#\#}P < 0.001$ *vs* control group.

3.6.8. EAF administration restores HMG-CoA/mevalonate ratios by inhibiting cholesterol biosynthesis in CCT diet-fed rats

The results indicated a significant ($P < 0.001$) increase in the HMG-Co A/mevalonate ratio in CCT diet-fed rats. The elevated HMG-CoA/mevalonate ratio in the livers of fasting rats was solely due to the reduced activity of the enzyme HMG-CoA reductase and not because of a decrease in the availability of nicotinamide adenine dinucleotide phosphate (NADPH), which is also necessary for the enzyme's activity. Furthermore, the administration of EAF to CCT diet-fed rats significantly ($P < 0.001$) decreased HMG-CoA reductase enzymatic activity by inhibiting cholesterol biosynthesis in the liver, as evident from a higher HMG-CoA/mevalonate ratio resembling that of the PC-treated group. The HMG-CoA/mevalonate ratios of the different animal groups are shown in Fig. 5F.

3.6.9. Regulatory effects of EAF on cholesterol metabolism-associated proteins in CCT diet-induced alterations

To understand the mechanism of EAF fraction in regulating cholesterol metabolism, we used immunoblotting techniques to analyze the expression of liver proteins, including ABCG1, LDL-R, LXRα, PPARγ, and SREBP-1. The resulting protein expression and quantification data were presented in Fig. 5G–K. EAF at 50 and 100 mg/kg p.o. significantly ($P < 0.001$) elevated the LDL-R levels compared to CCT diet-fed rats. As sterols inhibit the cleavage of SREBP-1, the CCT-diet-fed rats indicated a significant ($P < 0.001$) elevation in the SREBP-1 precursors. Groups T1 and T2 indicated a significant ($P < 0.001$) dose-dependent-downregulation of pre-SREBP-1 levels, comparable to those of healthy control. LXRα expression was also significantly ($P < 0.001$) upregulated in the T1 group fed with 50 mg/kg p.o. of EAF compared to the DC group. PPARγ levels were upregulated significantly ($P < 0.001$) on the administration of EAF at 50 mg/kg p.o. ABCG1 levels significantly ($P < 0.001$) declined in CCT-diet-fed rats. However, the administration of EAF resulted in significant ($P < 0.001$) upregulation of the ABCG1 expression levels.

3.7. Histopathological assessment of EAF on vascular, hepatic, cardiac, and renal integrity following CCT diet induction

The aorta was processed for routine H&E staining. The control aorta section indicated the three layers of the aorta wall: the tunica intima, tunica media, and tunica adventitia. It was observed that aorta sections of CCT-diet-fed rats were atherogenic, indicating adventitia infiltration of lipid-containing macrophages with partial compression of the surrounding tunica media. Superficial erosion was also observed from the lumen of the aorta and infiltration of cells (Fig. 6B). EAF indicated direct anti-atherogenic effects in the aorta, as the sections were relatively similar to those of the control section with well-defined aorta layers.

Significant fatty modifications were seen in the liver tissues of the DC group, as revealed by histopathologic examination findings (Fig. 6G). Vacuolated hepatocytes, fatty cysts, and nuclei pushed to the periphery indicated hepatocyte cholesterol buildup in response to the CCT diet. Following ATS therapy and the CCT diet in the PC group, it illustrated normal parenchymal organization with sporadic fat cells that resembled control hepatocytes (Fig. 6H). The effects of the CCT diet on cholesterol deposits were reduced with EAF therapy for the T1 and T2 groups, respectively (Fig. 6I and J). Cardiac tissues of animals fed with the CCT diet indicated changes in cellular morphology and interstitial diffuse fibrosis (Fig. 6L). Treatment with EAF restored normal cardiac cellular morphology, with nucleated cells similar to those of control indicated in Fig. 6N and O. Histopathology of kidney tissues indicated an infiltration of inflammatory cells and glomerulosclerosis in the CCT-diet-fed rats. On administration with EAF, the T1 and T2 groups indicated restoration of normal kidney architecture, comparable to those of the control and PC groups (Fig. 6P–T).

3.8. VER from EAF indicated stronger interactions with protein targets compared to ATS

After conducting pharmacophore-based mapping of VER and standard statin drug, ATS, by feeding the 3D Conformer SDF files

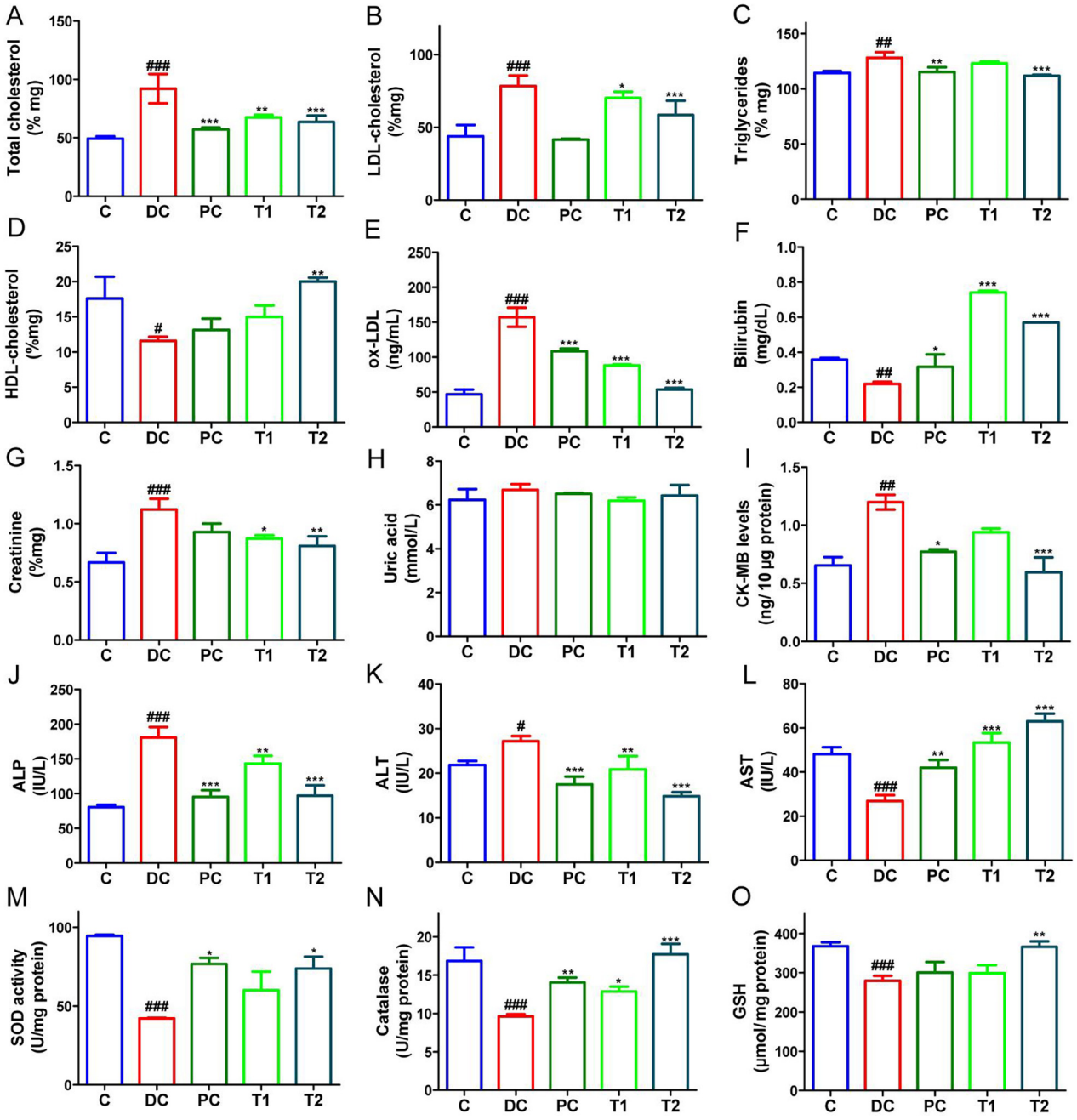

Fig. 4. Graphs indicating levels of (A) total cholesterol, (B) LDL-cholesterol, (C) triglyceride, (D) HDL-cholesterol, (E) ox-LDL, (F) bilirubin, (G) creatinine, (H) uric acid, (I) CK-MB levels, (J) ALP, (K) ALT, (L) AST, (M) superoxide dismutase (SOD), (N) catalase, and (O) glutathione peroxidase (GSH). Here, C (control pellet diet), DC (CCT diet), PC (CCT diet + positive control, Atorvastatin), T1 (CCT diet + EAF 50 mg/kg p.o.), T2 (CCT diet + EAF 100 mg/kg p.o). Values are expressed as means ± S.D. (n = 6). One-way ANOVA was performed, followed by Tukey's Post hoc test. $^{*}P < 0.05$, $^{**}P < 0.01$, $^{***}P < 0.001$ *vs* disease control group; $^{\#}P < 0.05$, $^{\#\#}P < 0.01$, $^{\#\#\#}P < 0.001$ *vs* control group.

into the PharmMapper engine, we successfully identified the pharmacological targets of VER/ATS in AS. The binding free energies (docking scores) and the interactions between the crucial amino acid residues and the ligands are illustrated in Fig. 7 and Table S3. The major phenolic compound in *C. glandulosum*, VER, demonstrated strong and stable interactions with oxysterol LXRβ (docking score –9.7) by binding with the SER^{242}, ASN^{239}-amino acid residues, HMG-CoA reductase (HMG-CoA R) (docking score –9.7) via hydrogen bond formation with ILE^{638}, SER^{637}, GLN^{648}, LYS^{633}amino acid residues, PPARγ (docking score –9.1) via hydrogen bond formation with GLU^{291}, GLU^{272}, GLN^{271} amino acid residues compared to the standard drug, ATS (LXRβ: docking score –7.7, HMG-CoA reductase: docking score –8.6, PPARγ: docking score –8.0). Similarly, VER also showed higher efficacy for ABCG1 (docking score –8.7) by interacting with VAL^{421}, LEU^{425}, PHE^{467}, and SER^{429} amino acid residues compared to ATS (ABCG1, docking score –7.0). For protein targets *viz*., iNOS and LXRα, VER indicated higher efficacies with iNOS (docking score –10.6) by interacting with CYS^{200}, GLY^{371}, VAL^{465} amino acid residues, and LXRα (docking score –9.1) by interacting with ARG^{367}, SER^{420}, SER^{416}, TRP^{441} amino acid residues. Consequently, the findings from the *in silico* analysis corresponded effectively with the *in vivo* results concerning the EAF and its principal phytoconstituent, VER.

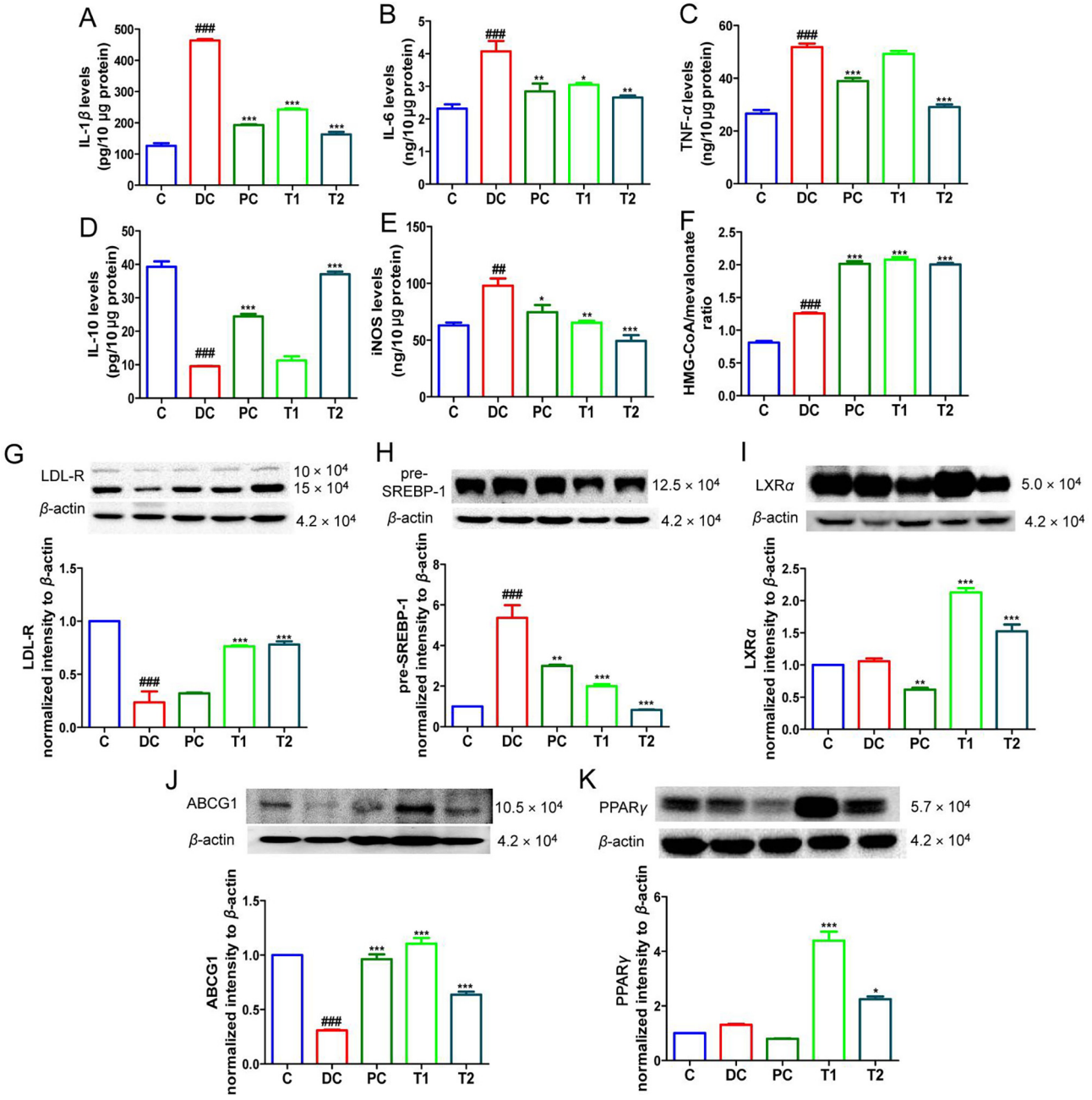

Fig. 5. Expression profiles of inflammatory cytokines in liver tissues, *viz*., (A) IL-1β, (B) IL-6, (C) TNF-α, (D) IL-10, and (E) iNOS levels as observed from ELISA; (F) hepatic HMG-CoA/mevalonate ratio; hepatic cholesterol metabolism associated proteins, *viz*., (G) LDL-R, (H) pre-SREBP-1, (I) LXRα, (J) ABCG1, and (K) PPARγ levels as observed from Western blotting analysis. Here, C (control pellet diet), DC (CCT diet), PC (CCT diet + positive control, atorvastatin), T1 (CCT diet + EAF 50 mg/kg p.o.) and T2 (CCT diet + EAF 100 mg/kg p.o). Values are expressed as means ± SD for six animals in each group. One-way ANOVA was performed, followed by Tukey's Post hoc test. $^{*}P < 0.05$, $^{**}P < 0.01$, $^{***}P < 0.001$ *vs* disease control group; $^{\#\#}P < 0.01$, $^{\#\#\#}P < 0.001$ *vs* control group.

4. Discussion

Statins are prescribed as over-the-counter medicines to lower cholesterol in patients suffering from cardiovascular diseases; nonetheless, the administration of statins is associated with a range of potential adverse effects, including the potential onset of diabetes mellitus (Pinal-Fernandez, Casal-Dominguez, & Mammen, 2018). Apart from the use of statins, there has been an exploration of the potential benefits of plant-based polyphenols in reducing the advancement of atherogenesis. *C. glandulosum* leaf extract has been reported to indicate ameliorative potential against hyperlipidemia and cardiovascular complications (Devi & Sharma, 2004; Jadeja et al., 2011; Khound & Devi, 2024). In this study, we performed bioactivity-guided fractionation of the hydro-methanolic leaf extract. During the preliminary evaluation of screening for enzyme-inhibitory potential, we found that the EAF indicated potent efficacy in lowering the breakdown of fats and carbohydrates. Pancreatic lipase plays a crucial role in the digestion of lipids. Lipid absorption can be diminished by inhibiting this enzyme, potentially helping to prevent obesity. Hypoglycemic agents commonly used in clinical settings, like acarbose, work by competitively inhibiting α-glucosidase in the small intestine's brush border. This action slows down the hydrolysis of carbohydrates, helping to reduce postprandial hyperglycemia (Costamagna et al., 2016). Different classes of naturally available phenolics, such as VER and luteolin, demonstrated non-

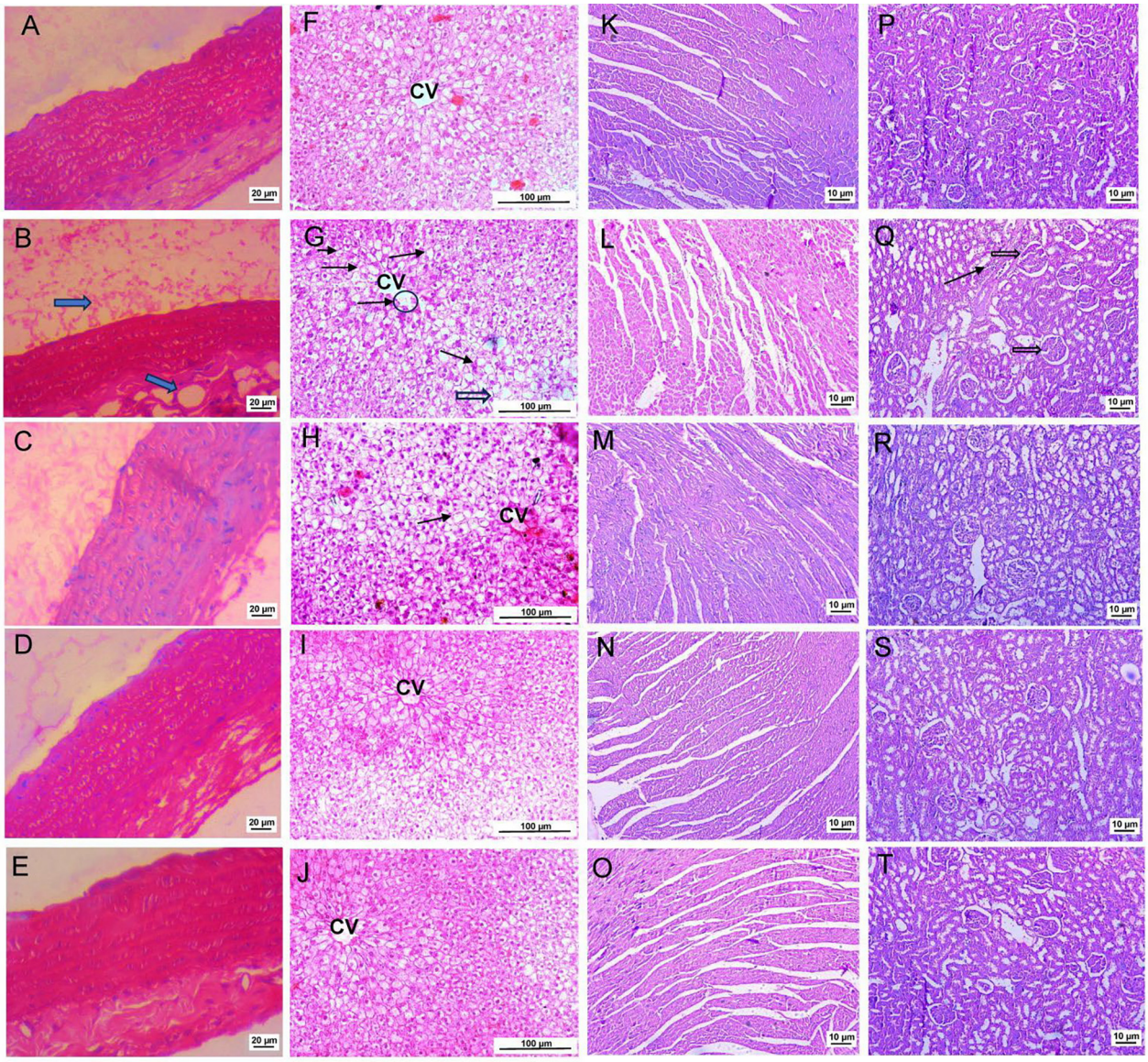

Fig. 6. Histopathology of H&E-stained aorta (×40, 20 µm) (A) Control showing normal histological structures of aorta including healthy aorta architecture; (B) CCT diet-induced group showing diseased condition with adventitia infiltrated with lipid-laden macrophages (foam cells) and rounded cells; (C) CCT diet treated with atorvastatin; (D and E) CCT diet with EAF treatment at 50 and 100 mg/kg p.o. doses showing effective recovery of aorta architecture similar to those of control group. H&E-stained liver (×20, 100 µm) (F) Control showing normal parenchymal structure; (G) CCT diet-induced group showing clusters of inflammatory cells (circled), and hypertrophic cell (open arrow); (H) CCT diet treated with atorvastatin, normal parenchymal structure with occasional fat cells (arrow); (I and J) CCT diet with EAF treatment at 50 and 100 mg/kg p.o. doses showing normal parenchymal structure. H&E-stained cardiac tissue (×10, 10 µm) (K) Control showing normal structure; (L) CCT diet-induced group with changes in cellular morphology and interstitial diffuse fibrosis; (M) CCT diet treated with atorvastatin; (N and O) CCT diet with EAF treatment at 50 and 100 mg/kg p.o. doses showing normal cardiac architecture. H&E-stained kidney tissue (×10, 10 µm) (P) Control showing normal structure with distinct glomeruli; Bowman's capsule (Q) CCT diet-induced group with infiltration of inflammatory cells (arrow) and glomerulosclerosis (open arrow); (R) CCT diet treated with atorvastatin; (S and T) CCT diet with EAF treatment at 50 and 100 mg/kg p.o. doses showing normal kidney architecture.

competitive inhibition of α-glucosidase and pancreatic lipase, leading to low levels of post-prandial glucose and reduced circulatory lipids levels that protect against inflammation, which in turn decreases the risks of atherogenesis (Costamagna et al., 2016; Martinez-Gonzalez et al., 2017). The occurrence of these phenolics in EAF, as observed by the phytochemistry, provided bioactivity against the digestive enzymes. Considering its bioactivity, EAF was undertaken for the phytochemical and further *in vitro* and *in vivo* evaluation. Phenolics and flavonoids are one of the major classes of phytochemicals associated with anti-atherosclerotic and hypolipidemic activity. By utilizing sophisticated analytical techniques, including chromatography and mass spectrometry, we aimed to elucidate the chemical composition of EAF and identify the potential bioactive molecules responsible for its pharmacological effects. Overall, the HR-LCMS analysis of EAF highlighted its rich chemical composition and diverse array of bioactive molecules such as VER, luteolin, apigenin, hispidulin, scutellarin, kaempferol, naringenin, many of which were previously reported for their pharmacological properties (Alipieva, Korkina, Orhan, & Georgiev, 2014; Dong, Huang, Shi, Xu, & Mang, 2021; Li, Zhou, Ji, Liang, & Xie, 2022; Wang & Ma, 2018). The current study further confirmed that VER is the principal compound present in the EAF, which was about 28% of the fraction, which has been previously reported in one of our studies investigating the antioxidant and cardioprotective properties of this plant (Khound et al., 2023). VER has been previously reported to exert an anti-atherosclerotic effect by regu-

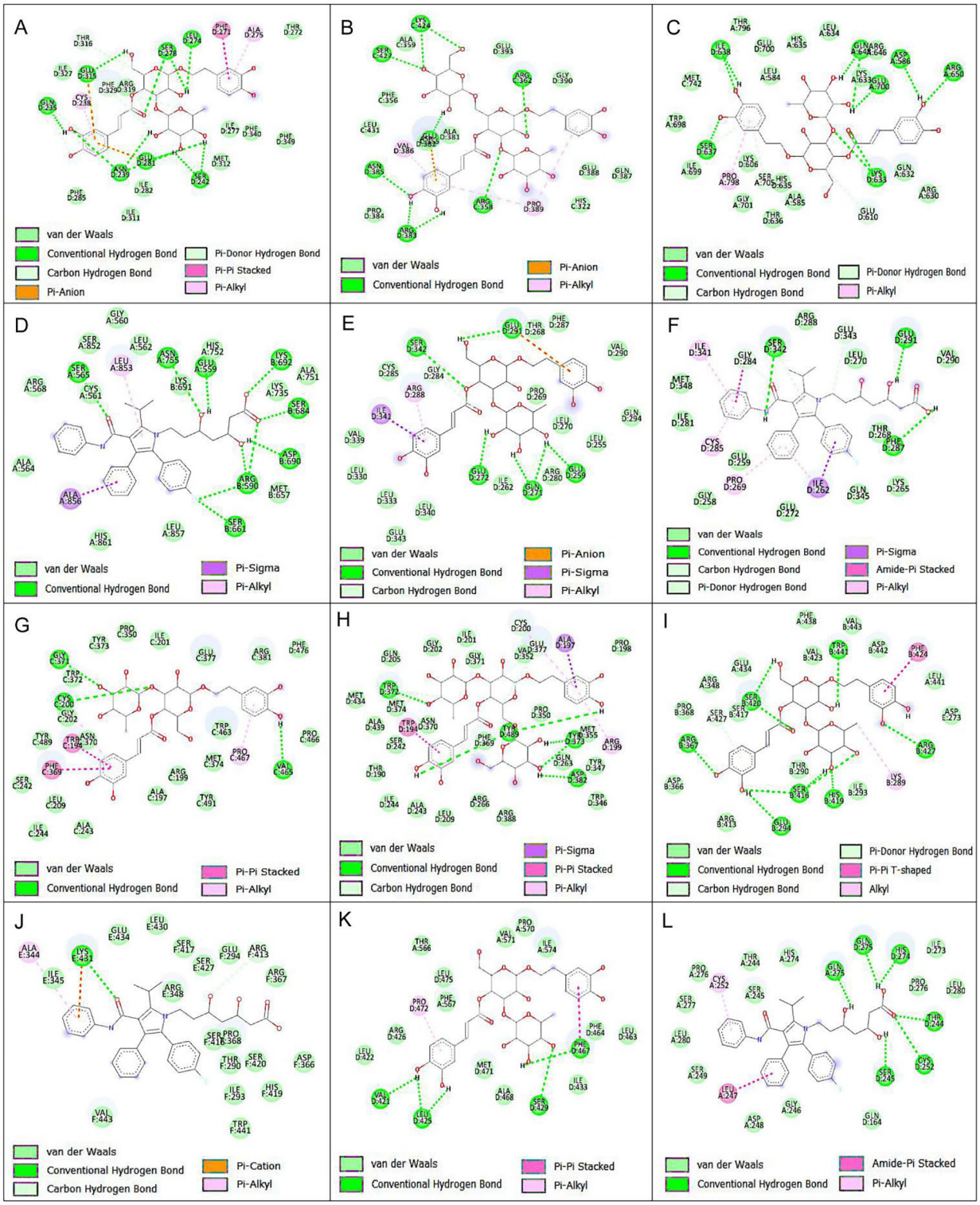

Fig. 7. Molecular docking analysis revealing interactions between essential amino acid residues of each protein and their corresponding ligands. (A) LXRβ (1PQ9)-VER (B) LXRβ (1PQ9)-ATS; (C) HMG-CoA R (2Q6C)-VER; (D) HMG-CoA R (2Q6C)-ATS; (E) PPARγ (1FM6)-VER; (F) PPARγ (1FM6)-ATS; (G) iNOS (1NSI)-VER; (H) iNOS (1NSI)-ATS; (I) LXRα (2ACL)-VER; (J) LXRα (2ACL)-ATS; (K) ABCG1 (7FDV)-VER; (L) ABCG1 (7FDV)-ATS protein–ligand complexes.

lating liver glycerophospholipid metabolism (Lei et al., 2023). It is a phenylethanoid glycoside found in various plants, including *Clerodendrum* species (Wang et al., 2018). This study aimed at the potential role of EAF in preventing AS, a condition characterized by the buildup of plaque in arteries, which can lead to cardiovascular diseases like heart attacks and strokes. The administration of EAF indicated a protective effect against the inflammatory changes induced by LPS-induced macrophages *in vitro* and the CCT diet *in vivo*. *C. glandulosum* extract has been previously reported to attenuate macrophage differentiation *in vitro* and lower chemoattractant and cell adhesion proteins in the thoracic aorta of atherogenic diet-fed rats (Jadeja et al., 2012). On activation, endothelial

cells commonly produce chemo-attractant cytokines, including monocyte chemoattractant protein-1, macrophage colony-stimulating factor, IL-6, TNF-α, and various cell adhesion molecules. This process attracts monocytes and lymphocytes, facilitating the adhesion of leukocytes to the endothelial surface (Loftus, 2011). Our study on evaluation for endothelial-to-monocyte cellular adhesion *in vitro* exhibited an inhibition of adhesion during treatment with EAF, thus indicating a lowered expression of cell adhesion molecules in endothelial cells on treatment with the EAF.

Oxidative stress and inflammation play crucial roles in the initiation and progression of AS. *C. glandulosum* extract, and its fractions have been reported to indicate antioxidant potentials both *in vitro* and *in vivo* (Devi, Banerjee, Sood, & Maulik, 2003; Doley, Singh, Devi, Singh, & Thokchom, 2016; Khound et al., 2023). In the present study, EAF was indicative of preventing the oxidative damage to hepatic tissue, thereby mitigating the deleterious effects of oxidative stress by augmenting the intricate antioxidant defense system comprising enzymatic antioxidants *viz*., SOD, catalase, GSH to maintain redox homeostasis and protect against oxidative injury, in CCT-diet induced atherogenic rats. This enhancement involves upregulation of antioxidant enzyme activity, replenishment of antioxidant reserves, or direct scavenging of ROS by bioactive constituents present in EAF, chiefly VER (Alipieva et al., 2014; Hsieh, Yu, Chu, & Hsieh, 2021; Shi et al., 1999). The liver, a major lipid metabolism and detoxification organ, is particularly susceptible to oxidative damage induced by high-fat diets such as the CCT diet (Deepa & Varalakshmi, 2004). Ox-LDL is closely associated with the development of AS, as lipids are susceptible to oxidation in the presence of ROS, resulting in their production (Duan et al., 2023). Excessive ox-LDL is taken up by macrophages, leading to the formation of foam cells that accumulate in blood vessels and accelerate AS development (Duan et al., 2023). Therefore, our results suggesting the decline in ox-LDL levels on EAF administration is a viable approach to prevent foam cell formation and improve cholesterol metabolism. Remarkably, treatment with EAF also effectively counteracts the inflammatory changes induced by the CCT diet in a dose-dependent manner. These observations are consistent with the notion that diets high in cholesterol and cholic acid can trigger inflammatory responses in the body, characterized by an imbalance between pro-inflammatory and anti-inflammatory signaling pathways. Pro-inflammatory cytokines such as IL-1β, IL-6, and TNF-α promote inflammation and contribute to the pathogenesis of various inflammatory diseases, including AS (Medzhitov, 2008). Conversely, IL-10 is crucial in dampening inflammation and promoting tissue repair and regeneration (Medzhitov, 2008). The elevation of iNOS levels in response to the CCT diet suggests increased production of nitric oxide (NO), a key mediator of inflammation; iNOS is an enzyme that catalyzes the production of NO from L-arginine that can act as a signaling molecule in inflammation and immune responses (Zamora, Vodovotz, & Billiar, 2000). Elevated NO levels can exacerbate inflammatory processes and contribute to tissue damage (Zamora et al., 2000). Therefore, by bolstering the liver antioxidant capacity, EAF helped alleviate oxidative damage induced by the CCT diet, thereby mitigating inflammation, lipid peroxidation, and cellular dysfunction associated with oxidative stress.

Liver enzymes such as ALP, ALT, and AST are markers of liver function and are released into the bloodstream when liver cells are damaged or inflamed. Elevated levels of these enzymes indicate liver injury and dysfunction, which can result from various factors, including metabolic disorders, inflammation, and toxicity (Giannini, Testa, & Savarino, 2005). The normalization of liver enzyme levels with EAF administration suggests that EAF may help preserve liver function and prevent hepatotoxicity associated with the CCT diet. Also, the normalization of bilirubin and creatinine levels with EAF administration suggests liver and kidney function improvements, which are important for overall metabolic health.

Our results indicated a stabilization of the dysbalanced lipid profile in CCT-diet-fed rats on treatment with EAF in the T1 and T2 groups, comparable to those of the PC group. Prior studies using *C. glandulosum* extracts and fractions indicated a decline in increased fecal cholesterol levels (Khound & Devi, 2024). The increased excretion of coprostan-3-ol and cholestane-3-ol indicated that EAF administration enhanced the elimination of cholesterol from the bodies of treatment groups T1 and T2. Therefore, the normalization of the lipid profile of the rats treated with EAF can be attributed to the mechanistic pathway of cholesterol metabolism and its elimination in feces. Therefore, in the present study, a comparison of the fecal metabolites of the different animal groups corroborated and validated the efficacy of the EAF fraction.

Hypercholesterolemia and cardiovascular diseases represent significant health concerns. One strategy to manage high cholesterol levels is to utilize medications that inhibit enzymes critical to cholesterol production. Among these, HMG-CoA reductase is pivotal, as it facilitates the key step in cholesterol synthesis. By blocking this enzyme, cholesterol production in liver cells decreases, boosting LDL-R expression.

Western blotting studies of the metabolic pathways also indicate the potential of EAF to enhance the elimination of cholesterol metabolites. Inhibition of HMG-CoA reductase induces LDL-R expression in the liver, lowering plasma cholesterol concentration (Kostner et al., 1989). Our findings on EAF-treated animals exhibited reduced HMG-CoA reductase activity and plasma cholesterol, leading to elevated LDL-R expression in the liver. As LDL-R plays a crucial role in regulating cholesterol homeostasis by facilitating the uptake of LDL cholesterol from the bloodstream into cells, particularly hepatocytes, this process helps maintain optimal cholesterol levels by removing excess LDL cholesterol from circulation through receptor-mediated endocytosis, thus reducing the risk of AS and cardiovascular diseases associated with high LDL cholesterol levels (Gong et al., 2023). Decreased LDL-R expression or function can lead to elevated LDL cholesterol levels and an increased risk of premature cardiovascular diseases (Sut et al., 2022). By upregulating LDL-R expression, EAF enhanced the clearance of LDL cholesterol from the bloodstream, thereby reducing LDL cholesterol levels.

SREBP-1 is synthesized as a precursor (1.25×10^6) attached to the nuclear envelope and endoplasmic reticulum (Xu, Nakamura, Cho, & Clarke, 1999). Mature SREBP-1 bands were not detected on visualization, indicating the presence of SREBP-1 s in their precursor forms. Under normal physiological conditions and sterol-depleted cells, SREBP-1 exists in an inactive precursor form that undergoes proteolytic cleavage to generate the mature, active form, which then translocates to the nucleus and activates the transcription of target genes involved in lipid synthesis (Sakai, Nohturfft, Goldstein, & Brown, 1998). The observed significant elevation in SREBP-1 precursors in CCT diet-fed rats suggests the dysregulation of lipid metabolism, particularly in the context of fatty acid and triglyceride synthesis, as sterols impede the cleavage process of SREBP-1 (Zelcer, Hong, Boyadjian, & Tontonoz, 2009). The significant elevation in SREBP-1 precursors might indicate increased activation of the SREBP-1 pathway, leading to the enhanced liver synthesis of fatty acids and triglycerides. A previous study reported that the expression of SREBP-1 in epididymal adipose tissue was decreased when HFD-fed mice were supplemented with *C. glandulosum* extract. (Jadeja et al., 2011). Present findings align with this: we observed a significant ($P < 0.05$) reduction in SREBP-1 levels in the animal groups receiving EAF at 50 and 100 mg/kg p.o doses.

PPARγ has been shown to indicate anti-atherosclerotic potential by playing a crucial role in promoting cholesterol efflux (Yin, Wang, Shi, Ji, & Liu, 2022). Notably, EAF-treated groups (T1 and T2) exhibited a greater increase in PPARγ levels compared to the diseased group, indicating that the bioactive fraction, EAF, contributed to this upregulation. PPARγ activates the PPARγ/LXRα

pathway, stimulating the expression of cholesterol efflux-related genes—ABCA1 and ABCG1 (Chawla et al., 2001; Lee, Park, Lee, & Hardwick, 2018; Yin et al., 2022). LXRs serve as sensors for sterols that protect the cells from excess cholesterol by promoting RCT and initiating its conversion to bile acids in the liver. LXRs, being nuclear receptors pivotal in controlling cholesterol and lipid metabolism, could potentially elicit anti-inflammatory and anti-atherogenic effects when specifically targeted (Calkin & Tontonoz, 2010). LXR agonists are considered potent antiatherogenic agents in rodent models of AS (Calkin & Tontonoz, 2010). Our findings of significant upregulation of LXRα levels in the treated group, T1, compared to those of the DC group, highlight its potential in promoting RCT and probable upregulation of ABCA1 and ABCG1 levels. The elevated levels of LXRα and ABCG1 transporter proteins in the liver reflected PPARγ-induced upregulation of LXRα that subsequently activated ABCA1 expression and promoted cholesterol efflux. Moreover, PPARγ may also facilitate the upregulation of ABCG1 by reducing cholesterol esterification, promoting HDL-dependent cholesterol efflux independently of the LXR pathway.

Valuable insight from the histological examination of the aorta sections indicated that the atherosclerotic lesions reduced significantly after EAF treatment in atherosclerotic rats. The sections from EAF-treated rats displayed structural features similar to those of the control group, with well-defined arterial wall layers. This suggests that EAF protects against AS by preserving the structural integrity of the arterial wall and preventing the infiltration of inflammatory cells and lipid deposition. Histopathological examination of the liver tissues revealed an accumulation of cholesterol within hepatocytes in response to the atherogenic diet (Parmar & Kar, 2007). The liver's intricate regulatory mechanisms maintain cholesterol balance in the body, ensuring that it remains within a healthy range. Dysfunction of the liver can lead to disturbances in cholesterol metabolism, potentially resulting in conditions such as hyper or hypocholesterolemia, which can have adverse health effects (Song, Liu, Zhao, Gao, & Zhao, 2021). The results of our study indicated reduced cholesterol deposits in the liver tissues on EAF treatment, comparable to the PC group treated with ATS drug known for its cholesterol-lowering effects. A significant decrease in CK-MB levels, a marker for heart damage, was observed in groups T1 and T2, indicating improved cardiac function on treatment with EAF in CCT-diet-fed rats. This correlated with the histological findings in the cardiac tissue of the T1 and T2 groups indicating reduced cellular lesions compared to those of the DC group.

Molecular docking studies indicate that the principal compound, VER, demonstrated significant interactions with various hepatic protein targets under investigation. Notably, the efficacy of VER presented in EAF surpassed that of the standard drug, ATS, as evidenced by a lower docking score. Thus, the *in-silico* analysis provides supportive evidence in conjunction with *in vitro* and *in vivo* studies regarding the ameliorative effects of EAF in managing AS in CCT-induced atherogenic rats.

5. Limitations of study

Our study has limitations. All natural compounds possess pleiotropic effects and multiple molecular and cellular targets. On the other hand, atherogenesis is a multifactorial condition and can have a multitude of mechanistic regulations, so sole modulation of reverse cholesterol transport, especially in complex organism systems, could not be sufficient in the prevention of AS. AS induced in Wistar albino rats utilizing CCT can only be correlated to early stages of AS, and therefore, mechanisms for the amelioration of later stages of AS are beyond the scope of this study and require further studies.

6. Conclusion

Our findings suggest that the EAF of the *C. glandulosum* leaf extract contains different bioactives, principally enriched with VER, that indicate potential therapeutic effects against DLD and AS. The VER-enriched EAF exhibited antioxidant and anti-inflammatory properties by reducing oxidative stress, inflammation, and atherogenic risk factors. Moreover, it regulated cholesterol and lipid metabolism by upregulation of ABCG1, LDL-R, LXRα, PPARγ, downregulation of SREBP-1 expression, and inhibition of lipid synthesis and accumulation. Histological analysis confirmed the protective effects of EAF supplementation on the structural integrity of the aorta and liver, heart, and kidney tissues. This suggests that EAF therapy could be a natural approach to prevention and management of cardiovascular disorders associated with DLD and AS. However, further research is needed to understand the specific mechanisms of action and the long-term effects of EAF supplementation in humans.

CRediT authorship contribution statement

Puspanjali Khound: Conceptualization, Data curation, Formal analysis, Investigation, Methodology, Writing – original draft, Writing – review & editing. **Nonibala Gurumayum:** Investigation. **Rajlakshmi Devi:** Funding acquisition, Supervision, Writing – review & editing.

Declaration of competing interest

The authors declare that they have no known competing financial interests or personal relationships that could have appeared to influence the work reported in this paper.

Acknowledgments

This work has been supported by the In-house core-funded research project (No. IASST/R&D/ICP/IHP-19/2023-24/1301-1310) of the Institute of Advanced Study in Science and Technology.

We sincerely acknowledge the Indian Council of Medical Research for the ICMR-SRF Fellowship granted to Ms. Puspanjali Khound (No. 45/04/2022/TRM/BMS), Sophisticated Analytical Instrument Centre, Institute of Advanced Study in Science and Technology, and the Department of Science and Technology, Government of India, for providing the necessary support. We would also like to acknowledge the Sophisticated Analytical Instrument Facility, the Indian Institute of Technology, Bombay (IIT Bombay) (SAIF), for conducting the HR-LCMS analysis.

Appendix A. Supplementary material

Supplementary data to this article can be found online at https://doi.org/10.1016/j.chmed.2025.02.007.

References

Alipieva, K., Korkina, L., Orhan, I. E., & Georgiev, M. I. (2014). Verbascoside—A review of its occurrence, (bio)synthesis and pharmacological significance. *Biotechnology Advances, 32*(6), 1065–1076.

Bergheanu, S. C., Bodde, M. C., & Jukema, J. W. (2017). Pathophysiology and treatment of atherosclerosis: Current view and future perspective on lipoprotein modification treatment. *Netherlands Heart Journal, 25*(4), 231–242.

Calkin, A. C., & Tontonoz, P. (2010). Liver x receptor signaling pathways and atherosclerosis. *Arteriosclerosis, Thrombosis, and Vascular Biology, 30*(8), 1513–1518.

Chawla, A., Boisvert, W. A., Lee, C. H., Laffitte, B. A., Barak, Y., Joseph, S. B., ... Tontonoz, P. (2001). A PPARγ-LXR-ABCA1 pathway in macrophages is involved in cholesterol efflux and atherogenesis. *Molecular Cell, 7*(1), 161–171.

Costamagna, M. S., Zampini, I. C., Alberto, M. R., Cuello, S., Torres, S., Pérez, J., ... Isla, M. I. (2016). Polyphenols rich fraction from *Geoffroea decorticans* fruits flour affects key enzymes involved in metabolic syndrome, oxidative stress and inflammatory process. *Food Chemistry, 190*, 392–402.

Costantino, H. R., Brown, S. H., & Kelly, R. M. (1990). Purification and characterization of an alpha-glucosidase from a hyperthermophilic archaebacterium, *Pyrococcus furiosus*, exhibiting a temperature optimum of 105 to 115 degrees C. *Journal of Bacteriology, 172*(7), 3654–3660.

Deepa, P. R., & Varalakshmi, P. (2004). Protective effects of certoparin sodium, a low molecular weight heparin derivative, in experimental atherosclerosis. *Clinica Chimica Acta, 339*(1–2), 105–115.

Devi, R., & Sharma, D. K. (2004). Hypolipidemic effect of different extracts of *Clerodendron colebrookianum* Walp in normal and high-fat diet fed rats. *Journal of Ethnopharmacology, 90*(1), 63–68.

Devi, R., Banerjee, S. K., Sood, S., & Maulik, S. K. (2003). *In-vitro* and *in-vivo* antioxidant activity of different extracts of the leaves of *Clerodendron colebrookianum* Walp in the rat. *Journal of Pharmacy and Pharmacology, 55*(12), 1681–1686.

Doley, P., Singh, A. V., Devi, N. M., Singh, C. B., & Thokchom, A. (2016). Reverse phase HPLC estimation of antioxidants and antimicrobial activities of *Clerodendrum colebrookianum* Walp. *Journal of Pharmacognosy and Phytochemistry, 5*(3), 199–205.

Dong, R., Huang, R., Shi, X., Xu, Z., & Mang, J. (2021). Exploration of the mechanism of luteolin against ischemic stroke based on network pharmacology, molecular docking and experimental verification. *Bioengineered, 12*(2), 12274–12293.

Duan, H., Song, P., Li, R., Su, H., & He, L. (2023). Attenuating lipid metabolism in atherosclerosis: The potential role of anti-oxidative effects on low-density lipoprotein of herbal medicines. *Frontiers in Pharmacology, 14*, 1161657.

Ellman, G. L. (1959). Tissue sulfhydryl groups. *Archives of Biochemistry and Biophysics, 82*(1), 70–77.

Giannini, E. G., Testa, R., & Savarino, V. (2005). Liver enzyme alteration: A guide for clinicians. *Canadian Medical Association Journal, 172*(3), 367–379.

Gong, K., Wang, M., Wang, D., Gao, Y., Ma, L., Yang, X., ... Han, J. (2023). Overexpression of NgBR inhibits high-fat diet-induced atherosclerosis in ApoE-deficiency mice. *Hepatology Communications, 7*(4), e0048.

Góth, L. (1991). A simple method for determination of serum catalase activity and revision of reference range. *Clinica Chimica Acta, 196*(2–3), 143–151.

He, C. P., Quan, W. J., Zeng, Y. L., Zhou, H. Y., You, P. D., Li, Z. X., ... Tuo, Q. H. (2023). Construction of nicotinic acid curcumin nanoparticles and its anti-atherosclerosis effect *via* PCSK9/LDL-R, ABCA1/Caveolin-1/LXR pathway. *Materials & Design, 229*, 111931.

Hsieh, P. F., Yu, C. C., Chu, P. M., & Hsieh, P. L. (2021). Verbascoside protects gingival cells against high glucose-induced oxidative stress *via* PKC/HMGB1/RAGE/NFκB pathway. *Antioxidants, 10*(9), 1445.

Im, S. S., & Osborne, T. F. (2011). Liver X receptors in atherosclerosis and inflammation. *Circulation Research, 108*(8), 996–1001.

Jadeja, R. N., Thounaojam, M. C., Ansarullah Devkar, R. V., & Ramachandran, A. V. (2010). *Clerodendron glandulosum* Coleb., Verbenaceae, ameliorates high fat diet-induced alteration in lipid and cholesterol metabolism in rats. *Revista Brasileira de Farmacognosia, 20*(1), 117–123.

Jadeja, R. N., Thounaojam, M. C., Ansarullah Jadav, S. V., Patel, M. D., Patel, D. K., ... Ramachandran, A. V. (2011). Toxicological evaluation and hepatoprotective potential of *Clerodendron glandulosum*. Coleb leaf extract. *Human and Experimental Toxicology, 30*(1), 63–70.

Jadeja, R. N., Thounaojam, M. C., Jain, M., Devkar, R. V., & Ramachandran, A. V. (2012). *Clerodendron glandulosum*. Coleb leaf extract attenuates *in vitro* macrophage differentiation and expression of VCAM-1 and P-selectin in thoracic aorta of atherogenic diet fed rats. *Immunopharmacology and Immunotoxicology, 34*(3), 443–453.

Jadeja, R. N., Thounaojam, M. C., Ramani, U. V., Devkar, R. V., & Ramachandran, A. V. (2011). Anti-obesity potential of *Clerodendron glandulosum*. Coleb leaf aqueous extract. *Journal of Ethnopharmacology, 135*(2), 338–343.

Joris, I., Zand, T., Nunnari, J. J., Krolikowski, F. J., & Majno, G. (1983). Studies on the pathogenesis of atherosclerosis. I. Adhesion and emigration of mononuclear cells in the aorta of hypercholesterolemic rats. *The American Journal of Pathology, 113*(3), 341–358.

Kalita, S., Singh, S. S., & Khan, M. L. (2012). *Clerodendrum colebrookianum* Walp.: A potential folk medicinal plant of North East India. *Asian Journal of Pharmaceutical and Biological Research, 2*(2), 256–261.

Khorrami, A., Ghanbarzadeh, S., Ziaee, M., Arami, S., Andalib, S., Maleki-Dizaji, N., & Garjani, A. (2014). Effects of LDL and oxidized LDL on cardiac function in isoproterenol-induced myocardial infarction in rat. *Drug Research, 64*(11), 576–583.

Khound, P., & Devi, R. (2024). *Clerodendrum glandulosum* Lindl.: A review of ethnopharmacology, pharmacological potentials, and their mechanism of action. *Chemistry & Biodiversity, 21*(4), e202302121.

Khound, P., Deb, P. K., Bhattacharjee, S., Medina, K. D., Sarma, P. P., Sarkar, B., & Devi, R. (2024). Phenolic enriched fraction of *Clerodendrum glandulosum* Lindl. leaf extract ameliorates hyperglycemia and oxidative stress in streptozotocin-nicotinamide induced diabetic rats. *Journal of Ayurveda and Integrative Medicine, 15*(3), 100906.

Khound, P., Sarma, H., Sarma, P. P., Jana, U. K., & Devi, R. (2023). Ultrasound-assisted extraction of verbascoside from *Clerodendrum glandulosum* leaves for analysis of antioxidant and antidiabetic activities. *ACS Omega, 8*(23), 20360–20369.

Kostner, G. M., Gavish, D., Leopold, B., Bolzano, K., Weintraub, M. S., & Breslow, J. L. (1989). HMG CoA reductase inhibitors lower LDL cholesterol without reducing Lp(a) levels. *Circulation, 80*(5), 1313–1319.

Lee, Y. K., Park, J. E., Lee, M., & Hardwick, J. P. (2018). Hepatic lipid homeostasis by peroxisome proliferator-activated receptor gamma 2. *Liver Research, 2*(4), 209–215.

Lei, P., Lü, J., Yao, T., Zhang, P., Chai, X., Wang, Y., & Jiang, M. (2023). Verbascoside exerts an anti-atherosclerotic effect by regulating liver glycerophospholipid metabolism. *Food Science and Human Wellness, 12*(6), 2314–2323.

Li, A. C., & Glass, C. K. (2004). PPAR- and LXR-dependent pathways controlling lipid metabolism and the development of atherosclerosis. *Journal of Lipid Research, 45*(12), 2161–2173.

Li, Z., Zhou, J., Ji, L., Liang, Y., & Xie, S. (2022). Recent advances in the pharmacological actions of apigenin, its complexes, and its derivatives. *Food Reviews International, 39*(9), 6568–6601.

Loftus, I. (2011). *Mechanisms of Vascular Disease*. In R. Fitridge & M. Thompson (Eds.), *Mechanisms of Vascular Disease: A Reference Book for Vascular Specialists* (pp. 43–63). Barr Smith Press.

Marklund, S., & Marklund, G. (1974). Involvement of the superoxide anion radical in the autoxidation of pyrogallol and a convenient assay for superoxide dismutase. *European Journal of Biochemistry, 47*(3), 469–474.

Martinez-Gonzalez, A. I., Díaz-Sánchez, Á. G., Rosa, L. A., Vargas-Requena, C. L., Bustos-Jaimes, I., & Alvarez-Parrilla, A. E. (2017). Polyphenolic compounds and digestive enzymes: *In vitro* non-covalent interactions. *Molecules, 22*(4), 669.

Medzhitov, R. (2008). Origin and physiological roles of inflammation. *Nature, 454*(7203), 428–435.

Nath, S. C., & Bordoloi, D. N. (1991). *Clerodendrum colebrookianum*, a folk remedy for the treatment of hypertension in northeastern India. *International Journal of Pharmacognosy, 29*(2), 127–129.

Parmar, H. S., & Kar, A. (2007). Protective role of *Citrus sinensis*, *Musa paradisiaca*, and *Punica granatum* peels against diet-induced atherosclerosis and thyroid dysfunctions in rats. *Nutrition Research, 27*(11), 710–718.

Pinal-Fernandez, I., Casal-Dominguez, M., & Mammen, A. L. (2018). Statins: Pros and cons. *Medicina Clinica, 150*(10), 398–402.

Rao, A. V., & Ramakrishnan, S. (1975). Indirect assessment of hydroxymethylglutaryl-CoA reductase (NADPH) activity in liver tissue. *Clinical Chemistry, 21*(10), 1523–1525.

Sakai, J., Nohturfft, A., Goldstein, J. L., & Brown, M. S. (1998). Cleavage of sterol regulatory element-binding proteins (SREBPs) at site-1 requires interaction with SREBP cleavage-activating protein evidence from in vivo competition study*. *The Journal of Biological Chemistry, 273*(10), 5785–5793.

Salunke, M. A., Wakure, B. S., & Wakte, P. S. (2023). High-resolution liquid chromatography and mass spectrometry (HR-LCMS) assisted phytochemical profiling and an assessment of anticancer activities of *Gracilaria foliifera* and *Turbinaria conoides* using *in vitro* and molecular docking analysis. *Journal of Biomolecular Structure & Dynamics, 41*(14), 6476–6491.

Sharma, N., Sharma, V. K., & Seo, S. Y. (2005). Screening of some medicinal plants for anti-lipase activity. *Journal of Ethnopharmacology, 97*(3), 453–456.

Shi, Y., Wang, W., Shi, Y., Jia, Z., Yao, S., Lin, W., ... Zheng, R. (1999). Fast repair of dAMP hydroxyl radical adduct by verbascoside *via* electron transfer. *Science in China Series C: Life Sciences, 42*(6), 621–627.

Song, Y., Liu, J., Zhao, K., Gao, L., & Zhao, J. (2021). Cholesterol-induced toxicity: An integrated view of the role of cholesterol in multiple diseases. *Cell Metabolism, 33*(10), 1911–1925.

Sut, S., Tahmasebi, A., Ferri, N., Ferrarese, I., Rossi, I., Panighel, G., ... Dall'Acqua, S. (2022). NMR, LC-MS characterization of *Rydingia michauxii* extracts, identification of natural products acting as modulators of LDLR and PCSK9. *Molecules, 27*(7), 2256.

Wang, J. H., Luan, F., He, X. D., Wang, Y., & Li, M. X. (2018). Traditional uses and pharmacological properties of *Clerodendrum* phytochemicals. *Journal of Traditional and Complementary Medicine, 8*(1), 24–38.

Wang, L., & Ma, Q. (2018). Clinical benefits and pharmacology of scutellarin: A comprehensive review. *Pharmacology & Therapeutics, 190*, 105–127.

Xie, J., Peng, L., Wang, T., Yang, C., Chen, N., Feng, X., ... Chen, Y. (2023). QiShenYiQi pill inhibits atherosclerosis by promoting reverse cholesterol transport PPARγ-LXRα/β-ABCA1 pathway. *Journal of Ethnopharmacology, 315*, 116684.

Xu, J., Nakamura, M. T., Cho, H. P., & Clarke, S. D. (1999). Sterol regulatory element binding protein-1 expression is suppressed by dietary polyunsaturated fatty acids. A mechanism for the coordinate suppression of lipogenic genes by polyunsaturated fats. *Journal of Biological Chemistry, 274*(33), 23577–23583.

Yang, H. X., Zhang, M., Long, S. Y., Tuo, Q. H., Tian, Y., Chen, J. X., ... Liao, D. F. (2020). Cholesterol in LDL receptor recycling and degradation. *Clinica Chimica Acta, 500*, 81–86.

Yang, H., Wang, J., Hou, A. J., Guo, Y. P., Lin, Z. W., & Sun, H. D. (2000). New steroids from *Clerodendrum colebrookianum*. *Fitoterapia, 71*(6), 641–648.

Yin, L., Wang, L., Shi, Z., Ji, X., & Liu, L. (2022). The role of peroxisome proliferator-activated receptor gamma and atherosclerosis: Post-translational modification and selective modulators. *Frontiers in Physiology, 13*, 826811.

Zamora, R., Vodovotz, Y., & Billiar, T. R. (2000). Inducible nitric oxide synthase and inflammatory diseases. *Molecular Medicine, 6*(5), 347–373.

Zelcer, N., Hong, C., Boyadjian, R., & Tontonoz, P. (2009). LXR regulates cholesterol uptake through Idol-dependent ubiquitination of the LDL receptor. *Science, 325*(5936), 100–104.